The advanced glycation end-product Nε-carboxymethyllysine promotes progression of pancreatic cancer: implications for diabetes-associated risk and its prevention

The advanced glycation endproduct N$^{\varepsilon}$-carboxymethyllysine promotes progression of pancreatic cancer: implications for diabetes-associated risk and its prevention

Running title: AGEs as diabetes-related risk factor for pancreatic cancer

Stefano Menini [1], Carla Iacobini [1], Luisa de Latouliere [1], Isabella Manni [2], Vittoria Ionta [1], Claudia Blasetti Fantauzzi [1], Carlo Pesce [3], Paola Cappello [4], Francesco Novelli [4], Giulia Piaggio [2], and Giuseppe Pugliese [1]*

[1] Department of Clinical and Molecular Medicine, "La Sapienza" University, Rome, Italy.

[2] Department of Research, Advanced Diagnostics, and Technological Innovation, Regina Elena National Cancer Institute, Rome, Italy.

[3] DINOGMI, University of Genoa Medical School, Genoa, Italy.

[4] Department of Molecular Biotechnology and Health Sciences, University of Turin, Turin, Italy.

***Corresponding author:**

Giuseppe PUGLIESE, M.D., Ph.D.

Department of Clinical and Molecular Medicine, Via di Grottarossa, 1035-1039 - 00189 Rome, Italy

Phone: +39-0633775440; Fax: +39-0633776327; E-mail: giuseppe.pugliese@uniroma1.it

Duality of interest: The Authors declare no conflicts of interest.

Word counts: abstract 300; text 4,000.

Number of figures and tables: 6 figures (+ 8 supplementary), 1 table (+3 supplementary).

Abstract

Diabetes is an established risk factor for pancreatic cancer (PaC), together with obesity, Western diet, and tobacco smoking. The common mechanistic link might be the accumulation of advanced glycation endproducts (AGEs), which characterizes all the above disease conditions and unhealthy habits. Surprisingly, however, the role of AGEs in PaC has not been examined yet, despite the evidence of a tumor-promoting role of RAGE, the receptor for AGEs. Here, we tested the hypothesis that AGEs promote PaC through RAGE activation. To this end, we investigated the effects of the AGE N^{ε}-carboxymethyllysine (CML) in human pancreatic ductal adenocarcinoma (PDA) cell lines and in a mouse model of *Kras*-driven PaC interbred with a bioluminescent model of proliferation. Tumor growth was monitored *in vivo* by bioluminescence imaging and confirmed by histology. CML promoted PDA cell growth and RAGE expression, in a concentration- and time-dependent manner, and activation of downstream tumorigenic signaling pathways. These effects were counteracted by RAGE antagonist peptide (RAP). Exogenous AGE administration to PaC-prone mice induced RAGE upregulation in pancreatic intraepithelial neoplasias (PanINs) and markedly accelerated progression to invasive PaC. At 11 weeks of age (6 weeks of CML treatment), PaC was observed in 8/11 (72.7%) of CML-treated versus 1/11 (9.1%) of vehicle-treated (Ctr) mice. RAP delayed PanIN development in Ctr mice but failed to prevent PaC promotion in CML-treated mice, likely due to competition with soluble RAGE for binding to AGEs and/or compensatory upregulation of the RAGE homolog CD166/ALCAM, which favored also tumor spread. These findings indicate that AGEs modulate the development and progression of PaC through receptor-mediated mechanisms and might be responsible for the additional risk conferred by diabetes and other conditions characterized by increased AGE accumulation. Finally, our data suggest that an AGE reduction strategy, instead of RAGE inhibition, might be suitable for risk management and prevention of PaC.

Key words: pancreatic cancer, Kras mutation, advanced glycation endproducts, RAGE, diabetes, bioluminescence imaging.

Introduction

Diabetes mellitus (DM), the prevalence of which is expected to increase dramatically in the next years (1), has been identified as a risk factor for a variety of malignancies, including pancreatic cancer (PaC) (2). The incidence of PaC continues to increase and it is predicted to become the second cause of cancer-related deaths in the US by 2030 (3). Since no effective therapy is available for the majority of patients and the 5-year survival is less than 7% (3), it is important to focus on prevention by eliminating risk factors

Studies designed to unravel the mechanistic link between DM and PaC are complicated by the fact that type 2 DM, the most common form of DM, could promote PaC through a variety of factors, including hyperglycemia itself, dyslipidemia, chronic inflammation, and insulin resistance/hyperinsulinemia (4-8). Recently, a tumor-promoting role has been suggested for the receptor for advanced glycation endproducts (RAGE), a single transmembrane receptor of the immunoglobulin superfamily. Ablation/blockade of this receptor was shown to slow down PaC development (9,10) by delaying progression of pancreatic intraepithelial neoplasia (PanIN) (10). Moreover, RAGE was found to regulate crosstalk between pro-survival pathways in pancreatic ductal adenocarcinoma (PDA) cells (11). RAGE interacts with multiple exogenous and endogenous ligands to induce inflammation (12) and is expressed in cell types implicated in tumor formation (13). As such, RAGE has been linked to cancer development/progression by facilitating the maintenance of a chronic inflammatory state (14) and/or promoting tumor growth (15). More specifically, RAGE ligation activates nuclear factor (NF)-κB, a critical transcription factor transducing a variety of inflammatory signals (16) and up-regulating RAGE itself, since the gene encoding RAGE contains functional NF-κB binding elements (17).

The name of RAGE derives from its ability to bind the advanced glycation end-products (AGEs). Though a role for AGEs has been tentatively proposed to explain the increased risk of various cancers (including PaC) in diabetic and obese individuals (18), surprisingly, their role in pancreatic carcinogenesis has never been investigated (19). AGEs are a heterogeneous group of compounds

(20) that accumulate in tissues of aging individuals and, at an accelerated rate, in diabetic and obese subjects, due to several mechanisms, including increased carbohydrate and lipid substrate availability, oxidative and non-oxidative conditions favoring the glycation process, and impaired detoxification (21). In addition to endogenous production, high-temperature processed foods and cigarette smoking are major environmental sources of AGEs (22,23), which might therefore be involved in the increased PaC risk associated with dietary and smoking habits (24). Consistently with the involvement of the AGE-RAGE axis in human PaC, a large prospective study reported that plasma levels of soluble RAGE (sRAGE), a truncated circulating form acting as a decoy receptor in preventing RAGE activation (25), were inversely associated with risk of PaC among Finnish male smokers (26).

This study aimed at investigating the tumor-promoting role of N^{ε}-carboxymethyllysine (CML), a major AGE found *in vivo* (27) and a known RAGE ligand (28), in a well-characterized genetically-engineered mouse model of human PaC and in PDA cell lines.

Materials and methods

Study design

The *in vitro* study was designed to investigate the tumor-promoting effects of CML on PDA cell lines by evaluating cell growth and the main tumorigenic pathways involved in PaC promotion. A secondary objective was to assess whether these effects were RAGE-mediated.

The *in vivo* study was designed to evaluate the effect of CML on progression of early murine pancreatic neoplasia. The primary and secondary endpoints were the development of invasive PaC and development/progression of PanINs, respectively. The number of mice was not pre-specified. According to the Ethics Committee recommendation, to limit the number of animals, the experiments were stopped when it was sufficient to confirm or reject the working hypothesis in a statistically and clinically meaningful manner. Biological samples were recoded by a technician (CC, see Acknowledgements) at the time of collection and analyzed by investigators blinded to group assignment. The research protocol was approved by the National Ethics Committee for Animal Experimentation of the Italian Minister of Health (Authorization n. 1470/2015-PR). The animals were housed in single cages and cared according to standards articulated in the "Animal Research: Reporting of In Vivo Experiments" (ARRIVE) (https://www.nc3rs.org.uk/arrive-guidelines) guidelines.

Cell lines

Human MIA PaCa-2 and PANC-1 (PDA) cells (Sigma-Aldrich, St.Louis, MO, USA) and the normal human pancreatic duct epithelial (HPDE) cell line HPDE-E6E76c7 (H6C7) (provided by Dr. Maurizio Fanciulli, Regina Elena National Cancer Institute, Rome, Italy) were maintained in DMEM supplemented with 10% fetal bovine serum and incubated with native human serum albumin (HSA, Sigma-Aldrich; vehicle, Ctr) or CML-modified HSA (1 μg/mL to 100 μg/mL, CML) ± the S100P-derived RAGE antagonist peptide (RAP, Calbiochem, Merck KGaA, Darmstadt, Germany; 10 μmol/L, daily added). CML was prepared as previously reported (21,29). Characterization of CML preparations by 2,4,6-trinitrobenzene sulfonic acid (TNBSA) revealed that

13.2±2.1% and 14.7±2.4% of total free amino groups (lysine and arginine) in CML-HSA and CML-MSA, respectively, were modified. This rate of modification was previously found to have an activity to bind RAGE (28), but not scavenger receptors (30) and is comparable to that detected in serum proteins of diabetic patients (31). RAGE binding to the CML-MSA preparation used in the *in vivo* studies was confirmed in a functional ELISA (Supplementary Figure 1). The RAP concentration was chosen on the ground of the available literature data (9). Detailed information on CML preparation, characterization, and RAGE-binding activity is provided as Supporting Information.

Cell viability and proliferation

Cell viability and proliferation were evaluated by cell count using Countess® Automated Cell Counter (Life Technologies Carlsbad, CA, USA) and a 3-(4,5-dimethylthiazol-2-yl)-2,5-diphenyltetrazolium bromide (MTT)-based cell proliferation assay (Roche Diagnostics GmbH Mannheim, Germany).

RAGE and molecular targets of tumorigenic signaling pathways in PDA cells

The mRNA expression of the genes coding for (a) RAGE; (b) CD166/ activated leukocyte cell adhesion molecule (ALCAM), a close structural and functional homolog of RAGE (32); (c) nuclear factor of activated T-cells cytoplasmic 1 (NFATC1) and serine/threonine-protein kinase Pim-1 (PIM1), two Signal Transducer and Activator of Transcription 3 (STAT-3) downstream targets which have been involved in inflammation-driven PaC (33); and (d) interleukin-6 (IL-6), the production of which was shown to be RAGE-dependent in KC mice (10) (*AGER*, *ALCAM*, *NFATC1*, *PIM1*, and *IL6*, respectively) was assessed by real-time (RT)-PCR using a StepOne Real-Time PCR System and the TaqMan Gene Expression assays (Applied Biosystems Monza, Italy) listed in Supplementary Table 1 (34,35).

Nuclear protein extracts were obtained from cells monolayers using the Nuclear Extract Kit (Active Motif Corp., Carlsbad, CA, USA). Nuclear protein levels of NF-κB p65, phosphorylated STAT3 (p-STAT3), NFATC1, and hypoxia-inducible factor 1 (HIF-1) α, which is involved in

RAGE-Kras promotion of PaC (10), were assessed by Western blot (see Supplementary Table 2 for antibodies). The DNA-binding activity of NF-κB/p65 and HIF-1α were assessed by the TransAM NFkB p65 and HIF-1 Kit, respectively (Active Motif Corp.). Details on RAGE neutralization experiments with an anti-RAGE antibody are provided as Supporting Information.

Transgenic animal model

The effect of CML administration on PaC development through RAGE activation was investigated in genetically-engineered mice *Pdx1-Cre;LSL-Kras*$^{G12D/+}$ (KC mice) on a C57Bl/6 background, that develop autochthonous lethal PaC in a pattern recapitulating human PDA with high fidelity (36). KC mice were interbred with *MITO-Luc* (for mitosis luciferase) reporter mice on a *FVB* background (37,38) to obtain KC-*Mito* (KCM) mice (see Supporting Information).

Five-week old KCM mice were randomly assigned to treatment with daily i.p. injections of 30 μg of native mouse serum albumin (MSA, Ctr) or CML-modified MSA (CML) (21). At this age, pancreatic parenchyma is histologically normal and early-stage PanINs are rarely observed (36,38). The treatment dose was chosen based on our previous data showing that this injection protocol results in a 2-to-3 fold increase in circulating and tissues AGE levels (21,39), similar to that observed in experimentally diabetic mice (29,34,40,41). We subjected Ctr and CML-treated mice to longitudinal *in vivo* BLI imaging and manual palpation of the abdomen to monitor tumor development. Additional groups of KCM mice were treated with RAP at the dose of 100 μg/day (9) in addition to native MSA (Ctr+RAP) or CML-MSA (CML+RAP).

***In vivo* imaging of cell proliferation in PaC**

Starting from the fifth week of age, *in vivo* imaging (37,38) was carried out every other week as previously reported (38). Briefly, 10 min after administration of D-luciferin (75 mg/kg body weight, i.p.; Perkin Elmer, Hopkinton, MA, USA), photon emission from the different body areas was acquired for 5 min and analyzed by a CCD camera (Xenogen IVIS Lumina System, Perkin Elmer). A specific region of interest (ROI) corresponding to the abdominal area occupied by the pancreas was manually selected and light emission from this ROI was evaluated with a Living Image

Software (Caliper Life Sciences, Perkin Elmer). Data were expressed as photon/second/cm^2/steradiant (p/s/cm^2/sr).

Ex vivo imaging

At the end of treatment, mice were anesthetized for the last *in vivo* imaging session and then euthanized by cervical dislocation. Pancreas was dissected and exposed to the CCD camera for 5 minutes for photon emission assessment.

Next, samples were partly frozen and kept at -80°C for molecular analysis and partly embedded in paraffin for histological analysis and immunohistochemistry (IHC).

Pancreas histology

At least six 4 μm-thick non-serial pancreatic sections were stained with hematoxylin and eosin, examined to confirm the presence of cancer or grade dysplastic ducts according to previously established criteria (36).

The KCM, as well as KC mice, develop with complete penetrance ductal lesions identical to all three stages of human PanINs (36,42). Number of low-grade (PanIN-1A/B) and high-grade (PanIN-2/3) dysplastic ducts were counted and expressed as a percentage of total ducts in the specimen (10).

Pancreatic protein levels of RAGE and CD166/ALCAM, co-localization of RAGE with CML, and phosphorylation status of STAT3

Pancreatic tissue distribution of RAGE and CD166/ALCAM was analyzed by IHC. Co-localization of RAGE and CML was analyzed by dual label immunofluorescence, as described in the Supporting Information. Pancreatic protein levels of p-STAT3, RAGE, and CD166/ALCAM were assessed by Western blot (see Supplementary Table 2 for antibodies).

For Western blot analysis, proteins were separated on a TGX Stain-Free Gel (Bio-Rad Laboratories, Hercules, California, USA), as detailed in the Supporting Information.

Serum levels of the AGE CML, sRAGE and IL-6

Serum levels of CML, sRAGE, and IL-6 were assessed using ELISA kits (Cell Biolabs Inc. San Diego, CA, USA, for CML; R&D Systems, Minneapolis, MN, USA, for sRAGE and IL-6) (34,35).

Lack of interference of circulating sRAGE and RAP with CML assay~~s,~~ and of CML and RAP with sRAGE assay was verified by adding increasing concentrations of each of these ligands to serum prior to perform the ELISAs (Supplemental Figure 2). Details of the experimental procedure are provided as Supporting Information.

Statistical analysis

Results are expressed as mean±SD and/or percentage.

Differences between cell types/treatments or animal groups were assessed using the Student's t test or the one-way ANOVA followed by the Student-Newman-Keuls test for multiple comparisons, as appropriate. Differences among animal groups in PaC prevalence at 11 weeks of age were assessed using the Fisher's exact test to compute a *P*-value from a contingency table. A *P*-value <0.05 was considered significant.

All statistical tests were performed on raw data, using SPSS 13.0 statistical software.

Results

The AGE CML promotes PDA cell proliferation and induces RAGE up-regulation

CML promoted proliferation of Mia PaCa-2 cells in a time- and concentration-dependent manner (Figure 1A-B). A dose-dependent induction of proliferation was observed also in PANC-1 cells, peaking at 10 μg/mL (Figure 1C), whereas HPDE cells responded only at the lowest concentration tested (Figure 1D).

Induction of proliferation was accompanied by increased RAGE expression in all three cell lines (Figure 1A-D). Interestingly, the CML concentration range with a positive dose-response relationship for proliferation at 24 hrs correlated with baseline RAGE expression (Figure 1E).

AGE/RAGE axis modulates tumorigenic pathways involved in PaC

CML treatment increased NK-κB p65 protein level and activation (Figure 2A-B) and p-STAT3 nuclear content (Figure 2A) and induced the transcriptional activity of the STAT3 target genes *NFATC1* and *PIM1* (Figure 2C).

RAP treatment counteracted all the molecular events elicited by CML and completely prevented CML-induced proliferation of PDA cells (Figure 2D). In addition, RAP blunted CML-induced nuclear translocation of HIF-1α and its DNA binding activity, nuclear translocation of NFATC1, activation of HIF-1α, and up-regulation of IL-6 (Supplementary Figure 3A-B). Proliferation and NF-κB nuclear translocation induced by CML were also inhibited by an anti-RAGE antibody in MIA PaCa-2 culture (Supplementary Figure 4A-B).

Expression of the RAGE homolog *ALCAM* (32) was not detectable (MIA PaCa-2) or at the limit of detectability (PANC-1) in PDA cells untreated or treated with CML or CML+RAP for 24 hrs.

CML favors development and progression of early murine PaC

After six weeks of CML treatment (i.e., at 11 weeks of age), more than half of KCM mice (6/11) showed positive abdominal imaging and ~1/4 (3/11) had a palpable abdominal mass (Figure 3A). At this age, only one Ctr-KCM mice showed significant abdominal photon emission

(Supplementary Figure 5). Therefore, to avoid loss of CML-treated KCM mice and limit the number of animals, the study was stopped at this time. However, since the i*n vivo* imaging does not allow to clearly identify the organ/tissue contributing to the BLI signal, we performed *ex vivo* imaging of the gastrointestinal apparatus at the time of the sacrifice, which confirmed that specific spots of BLI signals were mainly emitted by the pancreatic mass (Figure 3B).

At histological analysis, invasive PDA was confirmed in 8/11 (72.7%) CML-treated mice, compared with 1/11 (9.1%) Ctr mice (Table 1). Therefore, the majority of Ctr mice showed normal pancreatic architecture, though pre-invasive PanINs of various degrees were observed in all specimens analyzed (Figure 3C). Conversely, the majority of KCM mice treated with CML revealed a diffusely infiltrative PDA with well- and poorly-differentiated areas within the same tumor (Figure 3C-D); scattered low and high grade PanINs were also seen, especially at the tumor border (Figure 3E). These histological features were also observed in the pancreas from the one Ctr-KCM mice with invasive PaC, consistently with previous reports (33,34). No liver or lung metastases were observed grossly or in serial sections in both groups at this age (Table 1).

CML increases RAGE protein levels in PanINs and well-differentiated regions of invasive PaC of KCM mice

IHC for RAGE distribution in pancreatic sections of CML-treated KCM mice showed intense staining of PanINs, but not of the surrounding acinar tissue (Figure 4A-B). A cytoplasmic granular RAGE positivity was also observed in cells of duct-like structures in well-differentiated regions of the tumor, but not in surrounding undifferentiated areas (Figure 4C). Also PanINs of Ctr-KCM mice were positive for RAGE, though staining intensity was fainter than in CML-treated KCM mice and restricted to the apical/lateral border of PanIN cells (Figure 4D). Importantly, dual labeling immunofluorescence analysis showed co-localization of RAGE with CML in PanINs of CML-treated, but not of Ctr-KCM mice (Figure 4E).

Western blot analysis demonstrated higher RAGE levels in pancreatic specimens of CML-treated mice with well-differentiated PaC (Figure 4F) and significantly increased p-STAT3 levels in CML-treated- versus Ctr-KCM mice (Supplementary Figure 6).

RAP delays PanIN lesion development in Ctr-KCM mice but fails to prevent CML-induced PaC promotion and progression

As assessed by histological analysis, none of the ten KCM mice treated with RAP (Ctr+RAP) showed invasive PaC at 11 weeks of age (Table 1). However, quantitative analysis of neoplastic ducts showed that the number of low grade and, particularly, high grade PanIN lesions was significantly reduced in Ctr+RAP compared with Ctr-KCM mice (Figure 5).

Conversely, RAP administration did not counteract the promoting effect of CML on pancreatic tumorigenesis, as demonstrated by the high rate (6/7 animals, 87.5%) of invasive PaC observed in KCM mice treated with CML+RAP (Table 1). What is more, liver and/or lung metastases were observed grossly and confirmed by histological examination in 3/7 mice (42.5%) (Table 1 and Supplementary Figure 7).

Finally, Western blot analysis and IHC revealed a sharp increase of the protein level of the RAGE homolog CD166/ALCAM in mice treated with CML+RAP versus those receiving CML alone, but not in animals given RAP only (Figure 5D-E and Supplementary Figure 8).

RAP+CML treatment reduces serum levels of sRAGE and increases CML:sRAGE ratio

As expected, serum levels of CML were increased in KCM mice treated with CML and CML+RAP (Figure 6A). Conversely, serum sRAGE levels were strongly reduced by CML treatment, and further reduced by the combined CML+ RAP treatment (Figure 6B). As a result, the serum CML:sRAGE ratio (i.e., free or no sRAGE-associated CML) was higher in CML+RAP-treated than in CML-treated KCM mice (Figure 6C).

Consistently with a role of RAGE in IL-6 production, levels of this cytokine were increased in KCM mice treated with CML and were partly reduced by RAP treatment (Figure 6D).

Discussion

This study provides the first experimental evidence that the AGE CML (a) modulates the activity of signaling pathways involved in PaC development and stimulates cell proliferation in PDA cell lines in a RAGE-dependent manner; and (b) accelerates progression from PanINs to invasive PaC in a mouse model of *Kras*-driven PaC. Our results also support previous data demonstrating a permissive role for RAGE in early pancreatic neoplasia (10) and the efficacy of RAGE ablation/blockade in delaying PaC development in the presence of physiological levels of AGEs (9,10). However, our data argue against the utility of RAGE blockade/inhibition as a therapeutic option in conditions characterized by increased circulating AGE levels (22,23). Instead, they suggest that lowering AGE formation/level, rather than RAGE blockade, might represent a targeted risk reduction therapy for PaC in DM and other conditions characterized by increased AGE accumulation. The *in vitro* experiments demonstrated that CML stimulates proliferation of human PDA cell lines through RAGE activation, thus suggesting a role for the AGE/RAGE axis in PaC promotion. Several lines of evidence support this interpretation. Firstly, the time- and concentration-dependent stimulation of cell proliferation by CML was accompanied by a parallel up-regulation of RAGE expression and downstream tumorigenic pathways. Secondly, RAGE blockade with RAP counteracted the effects of CML on cell proliferation, NF-kB activation, STAT3 phosphorylation and up-regulation of its target genes. Thirdly, the higher was the basal expression of RAGE (i.e., MIA PaCa-2 > PANC-1 > HPDE), the larger was the range of CML concentration with a positive dose-response relationship for cell growth. This RAGE-dependent heterogeneity in the cell proliferative response to different AGE levels might represent one of the mechanisms through which DM promotes PaC. In fact, the high concentrations of AGEs characterizing DM may favor proliferation of initially transformed cells, which show a high expression level of RAGE, as compared to non-transformed cells, exhibiting a low level of this receptor.

The *in vivo* studies assessing the effect of CML on early pancreatic carcinogenesis showed that this AGE accelerates the development of PaC in KCM mice. Although a considerably degree of variability exists in total PaC burden among coeval mice, at 11 weeks of age , both KC (36,42) and KCM (38) mice showed a substantial number of PanIN lesions (~30% of pancreatic ducts), most of which of low-grade, and usually no invasive lesions. Therefore, the finding of 1/11 Ctr-KCM mouse with PaC should be considered as an occasional observation. Conversely, the finding that 8/11 CML-KCM mice presented with invasive PaC indicates that AGEs markedly accelerate PaC development. In addition, the content and distribution of RAGE protein and CML in pancreatic lesions strongly support the hypothesis that CML-enhanced tumorigenesis is mediated through RAGE expression and activation, in keeping with previous data showing that RAGE expression increases in parallel with progression of PanIN lesions in KC mice and is up-regulated in human PaC specimens (10). Moreover, the pronounced RAGE staining detected in cells of duct-like structures in well-differentiated regions of PaC, but not in the surrounding undifferentiated areas, suggests that RAGE is dispensable for subsequent steps of tumor progression. Taken together, these data support the hypothesis of a permissive role of RAGE for the progression of PanIN lesions to invasive PaC, as previously demonstrated in KC-RAGE knockout mice (10).

According with this assumption, we were able to demonstrate that RAGE blockade with RAP reduced the formation and progression of PanINs in KCM mice, consistent with a previous report in a pancreatic orthotopic model (9). However, one of the main aims of our study was to verify the hypothesis that blockade of the AGE/RAGE axis might represent a targeted risk reduction therapy for PaC in high-risk individual such as those with metabolic disorders and unhealthy lifestyle habits (2,26,43,44), who exhibit elevated circulating levels of AGEs (22,23). Contrary to our expectations, and at variance with data from cell culture studies and Ctr-KCM mice, RAGE blockade with RAP did not prevent the promoting effect of CML on pancreatic carcinogenesis and even favored tumor spreading and metastasis. These findings seem to argue against a role of the AGE-RAGE in the tumor-promoting effect of CML. However, two lines of evidence indicate they may have been related to two effects of RAP observed only when it was administered in mice with

pathological levels of CML (CML+RAP treatment). Firstly, the CML:sRAGE ratio (i.e., free CML) was higher in KCM mice treated with CML+RAP than in those treated with CML alone, a finding which suggests that, in the presence of high circulating CML levels, RAP has competed with CML for binding to sRAGE, thus reducing the decoy receptor activity of this circulating form of RAGE generated by both alternative splicing or ectodomain shedding of full-length RAGE. The resulting higher levels of free CML may have favored CML-induced tumor promotion. This interpretation is consistent with the concept that serum sRAGE levels represent a promising biomarker and therapeutic target in metabolic and neoplastic disorders (45,46).

Secondly, the protein levels of the RAGE homolog CD166/ALCAM (32) were higher in PaC specimens from KCM mice treated with CML+RAP than in those receiving only CML (and also those treated with RAP only). This finding suggests that, again only in the presence of high circulating levels of CML, RAGE blockade has resulted in AGE-induced up-regulation of CD166/ALCAM and/or favored the clonal expansion of PaC cells expressing this RAGE homolog (32). The finding that neither CML nor CML+RAP treatments of PDA cells for 24 hrs were able to modify basal *ALCAM* mRNA expression indicates that this is a gradual process involving *in vivo* tumor heterogeneity and clone selection. This interpretation is consistent with the observation that CD166/ALCAM shares with RAGE some endogenous ligands and is compensatory up-regulated after genetic deletion of its counterpart (32). In addition, it is supported by the finding that increased tumor levels of CD166/ALCAM in KCM mice treated with CML+RAP were associated with tumor spread, in keeping with the notions that this RAGE homolog is typically restricted to subsets of cells involved in dynamic growth and migration (47) and is an independent prognostic marker for poor survival and early tumor relapse in PaC (48). However, the findings in mice treated with CML+RAP should be confirmed in mice knockout for RAGE treated with CML, though, in our hands, RAP treatment provided similar protective effects to those induced by RAGE ablation in mice not treated with CML (10). Another limitation of our study is the lack of use of analytical techniques to confirm data on CML serum levels obtained by ELISA, though immunological and analytical methods were shown to produce comparable results in similar conditions (49).

In summary, our data demonstrate that the AGE/RAGE axis modulates PaC development in a genetically-engineered mouse model of the disease, as shown by the acceleration of PanIN progression to PaC and the concurrent up-regulation of RAGE expression induced by the AGE CML. This finding provides a conceivable molecular mechanism to explain the increased risk of PaC conferred by DM and other conditions of increased AGE accumulation. However, RAGE blockade with RAP was ineffective, if any, in protecting from CML-induced promotion of tumorigenesis, likely due to competition with sRAGE for binding to AGEs and compensatory up-regulation of CD166/ALCAM and/or clonal expansion of tumor cells expressing this RAGE homolog. Taken together, these results suggest that an AGE reduction strategy might be more suitable than RAGE blockade to reduce the PaC risk associated with DM, obesity, western diet and tobacco smoking.

Acknowledgements

This work was supported by a research grant from the Italian Association for Cancer Research (AIRC 2015; IG – 17640) to GP; AIRC 5 x mille 12182 and IG – 15257 to FN, University of Turin-Progetti Ateneo 2014-Compagnia di San Paolo (PANTHER to PC and PC-METAIMMUNOTHER to FN).

The Authors thank Cinzia Cataldo for technical assistance in sample collection, coding and histology processing.

Author Contributions: SM, CI and GP contributed to conception and design, acquisition of data, analysis and interpretation of data and drafting the article; CP, VI and CBF contributed to acquisition of histological, biochemical and molecular data; PC and FN provided the genetically-engineered *LSL-Kras*$^{G12D/+}$ and *Pdx-1-Cre* transgenic mice and contributed to critical revision of the article; GPi provided the genetically-engineered *MITO-Luc* mouse and contributed to design and interpretation of BLI data; LdL and IM performed *in vivo* and *ex vivo* imaging of cell proliferation. All authors gave final approval of the version to be published.

Non-standard abbreviations: DM = diabetes mellitus; PaC = pancreatic cancer; RAGE = receptor for advanced glycation endproducts; PanIn = pancreatic intraepithelial neoplasia; PDA = pancreatic ductal adenocarcinoma; NF-κB = nuclear factor-κB; sRAGE = soluble RAGE; CML = N^{ε}-carboxymethyllysine; HPDE = human pancreatic duct epithelial; HSA = human serum albumin; Ctr = HSA vehicle for in vitro experiments; RAP = RAGE antagonist peptide; MTT = 3-(4,5-dimethylthiazol-2-yl)-2,5-diphenyltetrazolium bromide; ALCAM = activated leukocyte cell adhesion molecule; NFATC1 = nuclear factor of activated T-cells cytoplasmic 1; PIM1 = serine/threonine-protein kinase Pim-1; IL6 = interleukin-6; RT-PCR = real-time-PCR; p-STAT3 = phosphorylated Signal Transducer and Activator of Transcription 3; HIF-1 = hypoxia-inducible factor 1; KC = *Pdx1-Cre;LSL-Kras*$^{G12D/+}$; *MITO-Luc* = mitosis luciferase; KCM = KC-*Mito*; BLI =

bioluminescence imaging; MSA = mouse serum albumin; Ctr = native MSA for in vivo experiments; ROI = region of interest; IHC = immunohistochemistry.

References

1. Boyle JP, Thompson TJ, Gregg EW, *et al*. Projection of the year 2050 burden of diabetes in the US adult population: dynamic modeling of incidence, mortality, and prediabetes prevalence. *Popul Health Metr.* 2010;8:8-29.
2. Huxley R, Ansary-Moghaddam A, Berrington de González A, *et al*. Type-II diabetes and pancreatic cancer: a meta-analysis of 36 studies. *BrJ Cancer.* 2005;92:2076-2083.
3. Rahib L, Smith BD, Aizenberg R, *et al*. Projecting cancer incidence and deaths to 2030: the unexpected burden of thyroid, liver, and pancreas cancers in the United States. *Cancer Res.* 2014;74:2913-2921.
4. Philip B., Roland CL, Daniluk J, *et al*. A high-fat diet activates oncogenic Kras and COX2 to induce development of pancreatic ductal adenocarcinoma in mice. *Gastroenterology* 2013;145:1449-1458.
5. Zechner D, Radecke T, Amme J, *et al*. Impact of diabetes type II and chronic inflammation on pancreatic cancer. *BMC Cancer* 2015;15:51.
6. Seshasai SR, Kaptoge S, Thompson A, *et al*. Diabetes mellitus, fasting glucose, and the risk of cause-specific death. *N Engl J Med.* 2011;364:829-841.
7. Stolzenberg-Solomon RZ, Graubard BI, *et al.* Insulin, glucose, insulin resistance and pancreatic cancer in male smokers. *JAMA 2005;*294:2872-2878.
8. Wang F, Herrington M, Larsson J, *et al*. The relationship between diabetes and pancreatic cancer. *Mol Cancer* 2003;6:2-4.
9. Arumugam T, Ramachandran V, Gomez SB, *et al*. S100P-derived RAGE antagonistic peptide reduces tumor growth and metastasis. *Clin Cancer. Res.* 2012;18:4356-4364.
10. Kang R, Loux T, Tang D, *et al*. The expression of the receptor for advanced glycation endproducts (RAGE) is permissive for early pancreatic neoplasia. *Proc Natl Acad Sc. USA.* 2012;109:7031-7036.

11. Kang R, Hou W, Zhang Q, *et al*. RAGE is essential for oncogenic KRAS-mediated hypoxic signaling in pancreatic cancer. *Cell Death Dis. 2014;*5:e1480.
12. Yao D, Brownlee M. Hyperglycemia-induced reactive oxygen species increase expression of the receptor for advanced glycation end products (RAGE) and RAGE ligands. *Diabetes* 2010;59:249-255.
13. Riehl A, Németh J, Angel P, *et al*. The receptor RAGE: Bridging inflammation and cancer. *Cell Commun Signal* 2009;7:12.
14. Gebhardt C, Riehl A, Durchdewald M, *et al*. RAGE signaling sustains inflammation and promotes tumor development. *J Exp Med.* 2008:205:275-285.
15. Taguchi A, Blood DC, del Toro G, *et al*.. Blockade of RAGE-amphoterin signalling suppresses tumour growth and metastases. *Nature* 2000;405:354-360.
16. Yan SD, Schmidt AM, Anderson GM, *et al*. Enhanced cellular oxidant stress by the interaction of advanced glycation endproducts with their receptors/binding proteins. *J Biol Chem.* 1994;269:9889-9897.
17. Li J, Schmidt AM. Characterization and functional analysis of the promoter of RAGE, the receptor for advanced glycation endproducts. *J Biol Chem.* 1997;272:16498-16506.
18. Yamagishi S, Nakamura K, Inoue H, *et al*. Possible participation of advanced glycation endproducts in the pathogenesis of colorectal cancer in diabetic patients. *Med Hypotheses* 2005;64:1208-1210.
19. Ahmad S, Khan H, Siddiqui Z, *et al.* AGEs, RAGEs and s-RAGE; friend or foe for cancer. *Semin Cancer Biol*. 2017 Jul 13. [Epub ahead of print]
20. Wautier JL, Schmidt AM. Protein glycation: a firm link to endothelial cell dysfunction. *Circ Res.* 2004;95:233-238.
21. Iacobini C, Menini S, Oddi G, *et al*. Galectin-3/AGE-receptor 3 knockout mice show accelerated AGE-induced glomerular injury: evidence for a protective role of galectin-3 as an AGE receptor. *FASEB J.* 2004;18:1773-1775.

22. Vlassara H. Advanced glycation in health and disease: role of the modern environment. *Ann N Y Acad Sci.* 2005;1043:452–460.
23. Cerami C, Founds H, Nicholl I, *et al*. Tobacco smoke is a source of toxic reactive glycation products. *Proc Nat Acad Sci USA*. 1997;94:13915–13920.
24. Anderson KA, Mack T, Silverman DT. Cancer Epidemiology and Prevention. In: Schottenfeld D, Fraumeni J, editors Pancreatic cancer. New York: Oxford University Press; 2006. p.741-742.
25. Kajikawa M, Nakashima A, Fujimura N, *et al*. Ratio of serum levels of AGEs to soluble form of RAGE is a predictor of endothelial function. *Diabetes Care* 2015;38:119-125.
26. Jiao L, Weinstein SJ, Albanes D, *et al*. Evidence that serum levels of the soluble receptor for advanced glycation endproducts are inversely associated with pancreatic cancer risk: a prospective study. *Cancer Res.* 2011;71:3582-3589.
27. Reddy S, Bichler J, Wells-Knecht KJ, *et al*. N-epsilon-(carboxymethyl)lysine is a dominant advanced glycation endproduct (AGE) antigen in tissue proteins. *Biochemistry* 1995;34:10872-10878.
28. Kislinger T, Fu C, Huber B, *et al*. N(epsilon)-(carboxymethyl)lysine adducts of proteins are ligands for receptor for advanced glycation endproducts that activate cell signaling pathways and modulate gene expression. *J Biol Chem.* 1999;274:31740-31749.
29. Iacobini C, Menini S, Blasetti Fantauzzi C, *et al*. FL-926-16, a novel bioavailable carnosinase-resistant carnosine derivative, prevents onset and stops progression of diabetic nephropathy in db/db mice. *Br J Pharmacol*. 2018;175:53-66.
30. Nagai R, Mera K, Nakajou K, *et al*. The ligand activity of AGE-proteins to scavenger receptors is dependent on their rate of modification by AGEs. *Biochim Biophys Acta*. 2007;1772:1192-1198.
31. Thornalley PJ, Argirova M, Ahmed N, *et al*. Mass spectrometric monitoring of albumin in uremia. *Kidney Int.* 2000;58:2228–2234.

32. von Bauer R, Oikonomou D, Sulaj A, *et al*. CD166/ALCAM mediates proinflammatory effects of S100B in delayed type hypersensitivity. *J Immunol.* 2013;191:369-377.
33. Menini S, Iacobini C, Ricci C, *et al*. Protection from diabetes-induced atherosclerosis and renal disease by D-carnosine-octylester: effects of early vs late inhibition of advanced glycation end-products in Apoe-null mice. *Diabetologia* 2015;58:845-853.
34. Iacobini C, Menini S, Ricci C, *et al*. Accelerated lipid-induced atherogenesis in galectin-3-deficient mice: role of lipoxidation via receptor-mediated mechanisms. *Arterioscler Thromb Vasc Biol.* 2009;29:831-836.
35. Baumgart S, Chen NM, Siveke JT, *et al*. Inflammation-induced NFATC1-STAT3 transcription complex promotes pancreatic cancer initiation by KrasG12D. *Cancer Discov.* 2014;4:688-701.
36. Hingorani SR, Petricoin EF, Maitra A, *et al*. Preinvasive and invasive ductal pancreatic cancer and its early detection in the mouse. *Cancer Cell* 2003;4:437-450.
37. Goeman F, Manni I, Artuso S, *et al*. Molecular imaging of nuclear factor-Y transcriptional activity maps proliferation sites in live animals. *Mol Biol Cell* 2012;23:1467-1474.
38. de Latouliere L, Manni I, Iacobini C, *et al*. A bioluminescent mouse model of proliferation to highlight early stages of pancreatic cancer: A suitable tool for preclinical studies. *Ann Anat* 2016;207:2-8.
39. Menini S, Iacobini C, Ricci C, *et al*. Ablation of the gene encoding p66Shc protects mice against AGE-induced glomerulopathy by preventing oxidant-dependent tissue injury and further AGE accumulation. *Diabetologia*. 2007;50:1997-2007.
40. Watson AM, Soro-Paavonen A, Sheehy K, Li J, *et al*. Delayed intervention with AGE inhibitors attenuates the progression of diabetes-accelerated atherosclerosis in diabetic apolipoprotein E knockout mice. *Diabetologia*. 2011;54:681-6899.
41. Lassila M, Seah KK, Allen TJ, *et al*. Accelerated nephropathy in diabetic apolipoprotein e-knockout mouse: role of advanced glycation end products. *J Am Soc Nephrol*. 2004;15:2125-2138.

42. Hingorani SR, Wang L, Multani AS, *et al*. Trp53R172H and KrasG12D cooperate to promote chromosomal instability and widely metastatic pancreatic ductal adenocarcinoma in mice. *Cancer Cell* 2005;7:469-483.
43. Larsson S C, Orsini N, Wolk A. Body mass index and pancreatic cancer risk: A meta-analysis of prospective studies. *I J C.* 2007;120:1993–1998.
44. Becker AE, Hernandez YG, Frucht H, *et al*. Pancreatic ductal adenocarcinoma: risk factors, screening, and early detection. *W J G* 2014;20:11182–11198.
45. Swart GW. Activated leukocyte cell adhesion molecule (CD166/ALCAM): developmental and mechanistic aspects of cell clustering and cell migration. *Eur J Cell Biol.* 2002;81:313-321.
46. Koyama H, Yamamoto H, Nishizawa Y. RAGE and soluble RAGE: potential therapeutic targets for cardiovascular diseases. *Mol Med.* 2007;13:625-635.
47. Tesarova P, Cabinakova M, Mikulova V, *et al*. RAGE and its ligands in cancer - culprits, biomarkers, or therapeutic targets? *Neoplasma* 2015;62:353-364.
48. Kahlert C, Weber H, Mogler C, *et al*. Increased expression of ALCAM/CD166 in pancreatic cancer is an independent prognostic marker for poor survival and early tumour relapse. *Br J Cancer* 2009;101:457-464.
49. Degenhardt TP, Grass L, Reddy S, *et al*. Technical note. The serum concentration of the advanced glycation end-product N epsilon-(carboxymethyl)lysine is increased in uremia. *Kidney Int*. 1997;52:1064-1067.
50. Ramji K, Kulesza DW, Chouaib S, *et al*. Off-target effects of plasmid-transcribed shRNAs on NFκB signaling pathway and cell survival of human melanoma cells. *Mol Biol Rep*. 2013;40:6977-6986.
51. Rao NV, Argyle B, Xu X, *et al*. Low anticoagulant heparin targets multiple sites of inflammation, suppresses heparin-induced thrombocytopenia, and inhibits interaction of RAGE with its ligands. *Am J Physiol Cell Physiol.* 2010;299:C97-110.
52. Menini S, Iacobini C, Ricci C, *et al*. The galectin-3/RAGE dyad modulates vascular osteogenesis in atherosclerosis. *Cardiovasc Res*. 2013;100:472-480.

Table 1. Pancreatic cancer (PaC) prevalence rate in KCM mice treated with MSA (Ctr), CML-modified MSA (CML), MSA plus RAP (Ctr+RAP) and CML plus RAP (CML+RAP) after 6 weeks of treatment (11 weeks of age).

Treatment	PaC N/tot	PaC %	P value	Metastasis N/tot
Ctr	1/11	9.1	—	0/11
CML	8/11	72.7	0.00752	0/11
Ctr+RAP	0/10	0	1	0/10
CML+RAP	6/7	85.7	0.00245	3/7 2 liver and 1 lung

KCM = *LSL-Kras$^{G12D/+}$;Pdx-1-Cre*;*MITO*; MSA = mouse serum albumin; CML = N$^{\varepsilon}$-carboxymethyllysine; RAP = RAGE antagonist peptide. N/tot = number of cases/total number of mice. *P* value = two-tailed *P* value for the difference in PaC rate vs. Ctr mice obtained from the Fisher's exact test.

Figure legends

Figure 1. CML induces PDA cell proliferation and RAGE up-regulation in a concentration- and time-dependent manner. Concentration (A) and time dependent (B) cell proliferation and *RAGE* expression in Mia PaCa-2 cells exposed to native HSA (Ctr) or CML-modified HSA (CML). Time dependent cell proliferation and *RAGE* expression in PANC-1 (C) and HPDE (D) exposed to 10 μg/ml of HSA or CML for 24 hrs, and relative representative images. Basal *RAGE* mRNA expression levels in Mia PaCa-2, PANC-1 and HPDE cells, as assessed by qRT-PCR (E). n = 5 wells per condition. Post-hoc multiple comparison: *P<0.01 vs. HSA; †P<0.001 vs. Mia PaCa-2; #P<0.001 vs. PANC-1. Dashed double arrow = range of CML concentration with a positive dose-response relationship for cell proliferation at 24 hrs.

Figure 2. CML activates the NF-κB/STAT3/Pim1/NFAT axis through RAGE signaling in PDA cell lines. Western blot for p65 NF-κB subunit and p-STAT3 protein expression in Mia PaCa-2 cells exposed to native HSA (Ctr), CML-modified HSA (CML) or CML+RAP at the concentration indicated for 24 and 48 hrs and relative band densitometry analysis from three separate experiments (A). NF-κB/p65 activity of the nuclear extracts assessed by ELISA (B). *PIM1* and *NFATC1* mRNA expression (C) and cell proliferation (D) in MIA PaCa-2 cells exposed to 50 μg/ml of HSA or CML, and 50 μg/ml of CML plus RAP 10 μmol/L for 24 hrs; n = 3 wells per condition. Post-hoc multiple comparison: *P< 0.01 vs. HSA; †P< 0.001 vs CML.

Figure 3. BLI and pancreatic histological analysis in Ctr and CML-treated KCM mice. *In vivo* (A, total body) and *ex vivo* (B, middle part of the gastrointestinal tract including the pancreas) BLI from a Ctr, tumor-free KCM mouse, and a CML-treated KCM mouse with invasive PaC, as assessed by histology. Different light emissions are highlighted with pseudo-colors based on the reported pseudo color scale, expressed in units of photon/second/cm^2/steradian (p/s/cm^2/sr). The corresponding histology of pancreatic sections stained with H&E (C): ten of eleven Ctr-KCM mice show normal pancreas histology of both acinar and islet (is) compartments, though PanINs (arrow)

of various degree were detected in all specimens analyzed (C, Ctr). The histological analysis of the pancreas from the majority (eight of eleven) of CML-treated KCM mice demonstrated a diffusely infiltrative adenocarcinoma (C, CML) with well (D, to the right of the dashed line) and poorly differentiated (D, to the left of the dashed line) regions within the same tumor. Scattered low and high grade PanINs (arrows) are recognizable, especially at the junction between normal acini (right part of panel E) and invasive PaC (left part of panel E). Scale bar = 100μm.

Figure 4. RAGE protein levels and tissue distribution and co-localization with CML in Ctr and CML-treated KCM mice. Intense positive staining for RAGE in PanINs (arrows) of CML-treated KCM mice (A); at higher magnification, intense positive staining on apical surface of columnar epithelial cells is observed, although a strong cytoplasmic granular positivity can also be appreciated (B). RAGE staining is also detectable in cells of duct-like structures in well-differentiated regions of the tumor (C), but not in surrounding undifferentiated areas (asterisks). Finally, faint staining for RAGE is also seen in PanINs (arrows) of Ctr-KCM mice (D). Scale bar = 100μm. Dual label immunofluorescence analysis shows positive staining for CML (green) and co-localization (yellow in the merged image) with RAGE (red) in PanIN lesions of CML-treated KCM mice. Conversely, in PanINs of Ctr-KCM mice CML is only barely detectable, whereas RAGE positivity, albeit fainter, is observable at the cell borders. Corresponding light microscopy images (H&E staining) have been included. Blue = DAPI (E). Representative Western blot (lower box) for RAGE protein expression in three tumor-free Ctr and three CML-treated KCM mice showing well-differentiated PaC at the histological examination (F); the upper box shows the acquisition of total protein content after Stain-Free gel exposure to ultraviolet light and protein transfer onto a nitrocellulose membrane.

Figure 5. PanINs in Ctr and Ctr+RAP KCM mice, and CD166/ALCAM protein levels in Ctr and CML-KCM mice treated or untreated with RAP. Percentages of normal (ND) and neoplastic ducts (LG and HG) by grade in ten Ctr (excluding the only Ctr mouse with PaC), and ten RAP-treated KCM mice (A). LG (low grade) = PainIN-1A plus 1B lesions; HG (high grade) =

PainIN 2 plus 3 lesions. Two-tailed test: *P< 0.001 vs. Ctr. Examples of HG PanINs-2 and 3 from a Ctr-KCM mouse (B): PanIN-2 lesion (left) with papillary architecture, revealing moderate loss of polarity, nuclear crowding and atypia; PanIN-3 lesion (right) shows more severe nuclear atypia, loss of polarity and budding off of small clusters of epithelial cells (arrow) into the lumen of the duct. Examples of LG PanINs-1A and 1B from a RAP-treated KCM mouse (C): three PanINs-1A (arrowheads) with a flat epithelial pattern, composed of tall columnar cells with basally located nuclei and abundant mucin content; PanIN-1B lesion (arrow) has similar cytological features but reveals a papillary/pseudostratified architecture. Representative Western blot for CD166/ALCAM in Ctr, CML, CML+RAP and Ctr+RAP-treated KCM mice and relative band densitometry analysis from seven mice per group (D). Normalization of the protein input was performed using the Stain-Free technology: after ultraviolet exposure of Stain-Free gel, proteins were transferred onto a nitrocellulose membrane and ultraviolet light-induced tryptophan fluorescence from the entire lane (i.e., total protein content) was measured; Stain-Free membrane for Western blot normalization is shown in Supplementary Fig. 5. CD166/ALCAM staining pattern in PaC from CML and CML+RAP-treated KCM mice (E); note the intense staining for CD166/ALCAM in the clusters of cells floating into the lumen of the duct-like structures (arrow) of CML+RAP-treated mice. Cells of surrounding undifferentiated areas were also positive for CD166/ALCAM (asterisk). Scale bar = 100μm. Post-hoc multiple comparison: *p<0.01 or **p<0.001 vs. Ctr; †p<0.01 vs. CML.

Figure 6. Serum levels of the AGE CML, sRAGE and IL-6. Serum levels of CML (A) and sRAGE (B), ratio of serum levels of AGEs to sRAGE (C) and IL-6 serum levels (D) in Ctr (n0 11), CML (n=11) and CML+RAP-treated (n=7) KCM mice. Post-hoc multiple comparison: *P< 0.01 and **P<0.001 vs. Ctr; †P<0.05 and ††P<0.01 vs. CML.

Figure 1

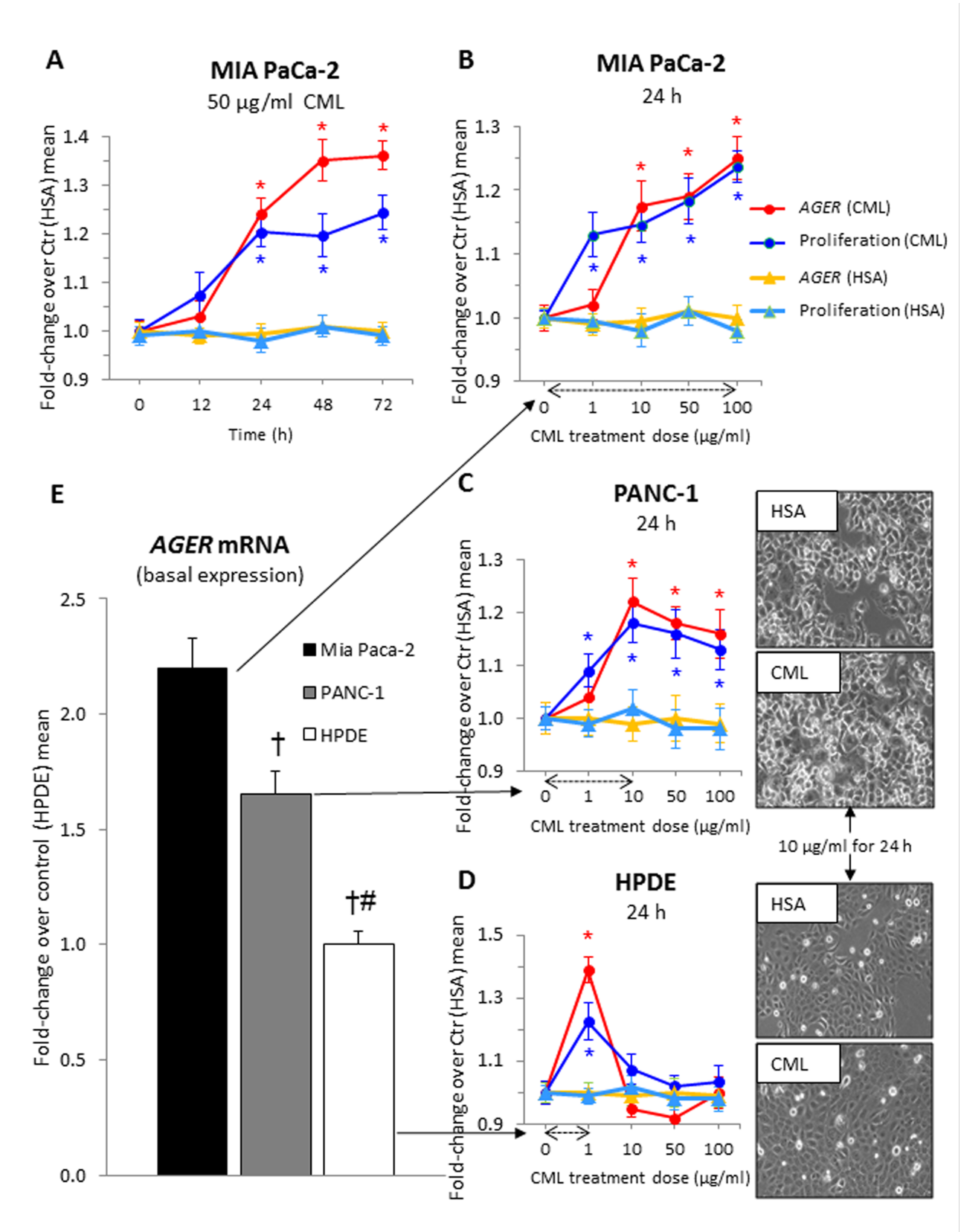
A
MIA PaCa-2
50 µg/ml CML
Fold-change over Ctr (HSA) mean
Time (h)
B
MIA PaCa-2
24 h
Fold-change over Ctr (HSA) mean
CML treatment dose (µg/ml)
AGER (CML)
Proliferation (CML)
AGER (HSA)
Proliferation (HSA)
C
PANC-1
24 h
Fold-change over Ctr (HSA) mean
CML treatment dose (µg/ml)
HSA
CML
10 µg/ml for 24 h
D
HPDE
24 h
Fold-change over Ctr (HSA) mean
CML treatment dose (µg/ml)
HSA
CML
E
AGER mRNA
(basal expression)
Fold-change over control (HPDE) mean
Mia Paca-2
PANC-1
HPDE

Figure 2

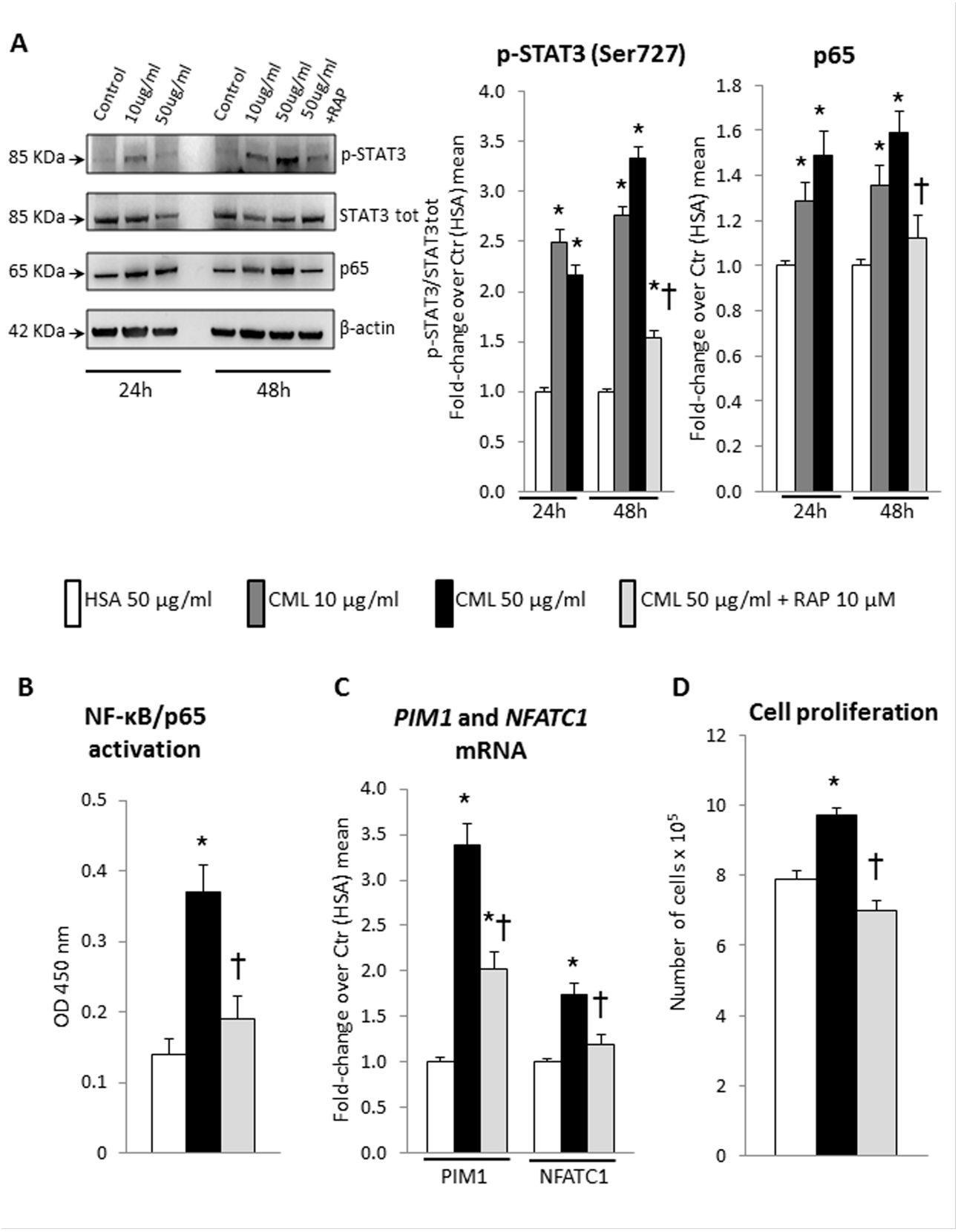
A
Control
10ug/ml
50ug/ml
Control
10ug/ml
50ug/ml
50ug/ml +RAP
85 KDa
p-STAT3
85 KDa
STAT3 tot
65 KDa
p65
42 KDa
β-actin
24h
48h
p-STAT3 (Ser727)
p-STAT3/STAT3tot
Fold-change over Ctr (HSA) mean
p65
Fold-change over Ctr (HSA) mean
HSA 50 µg/ml
CML 10 µg/ml
CML 50 µg/ml
CML 50 µg/ml + RAP 10 µM
B
NF-κB/p65 activation
OD 450 nm
C
PIM1 and NFATC1 mRNA
Fold-change over Ctr (HSA) mean
PIM1
NFATC1
D
Cell proliferation
Number of cells x 10^5

Figure 3

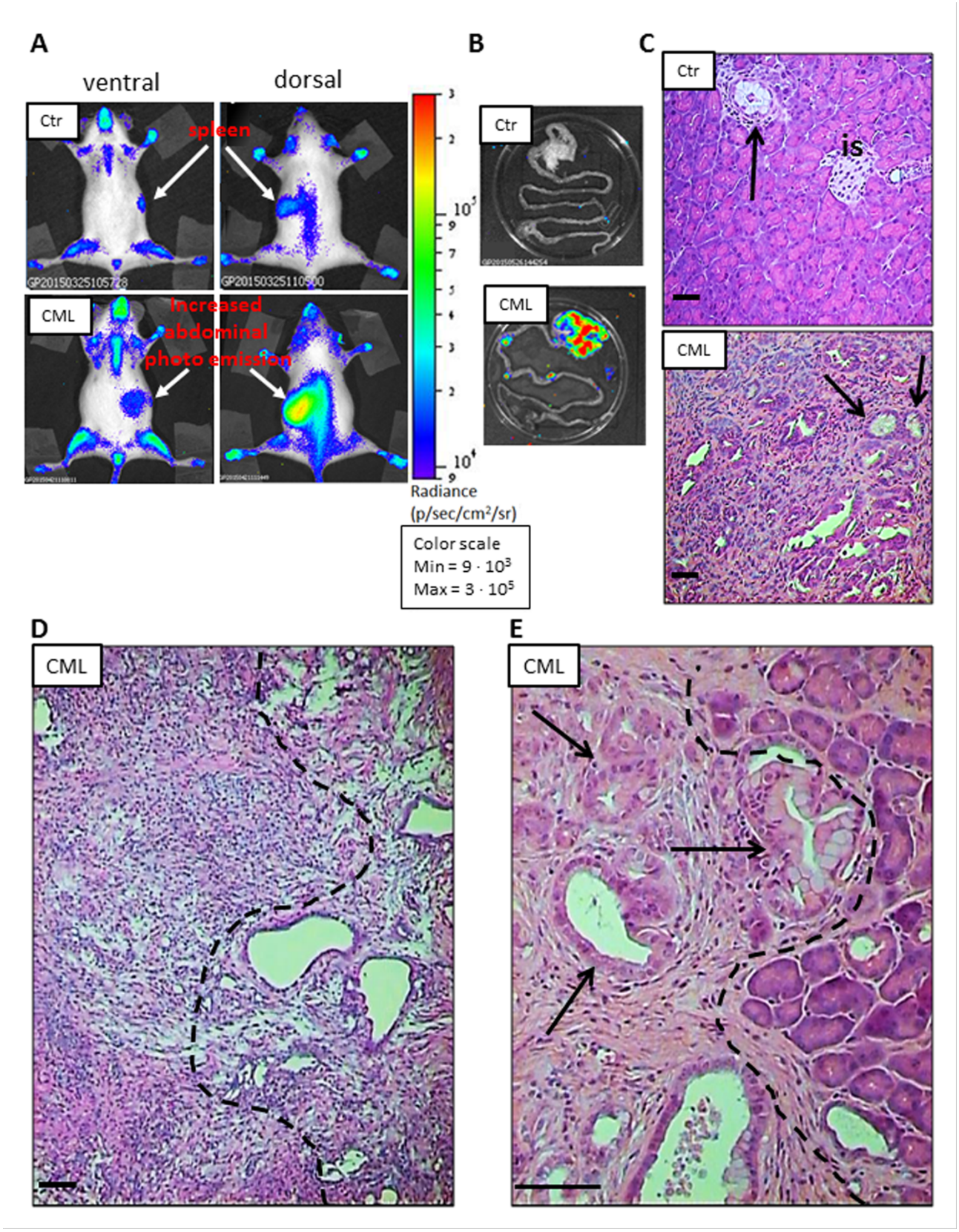
A
ventral
dorsal
Ctr
spleen
CML
Increased
abdominal
photo emission
Radiance
(p/sec/cm²/sr)
Color scale
Min = 9 · 10³
Max = 3 · 10⁵
B
Ctr
CML
C
Ctr
is
CML
D
CML
E
CML

Figure 4

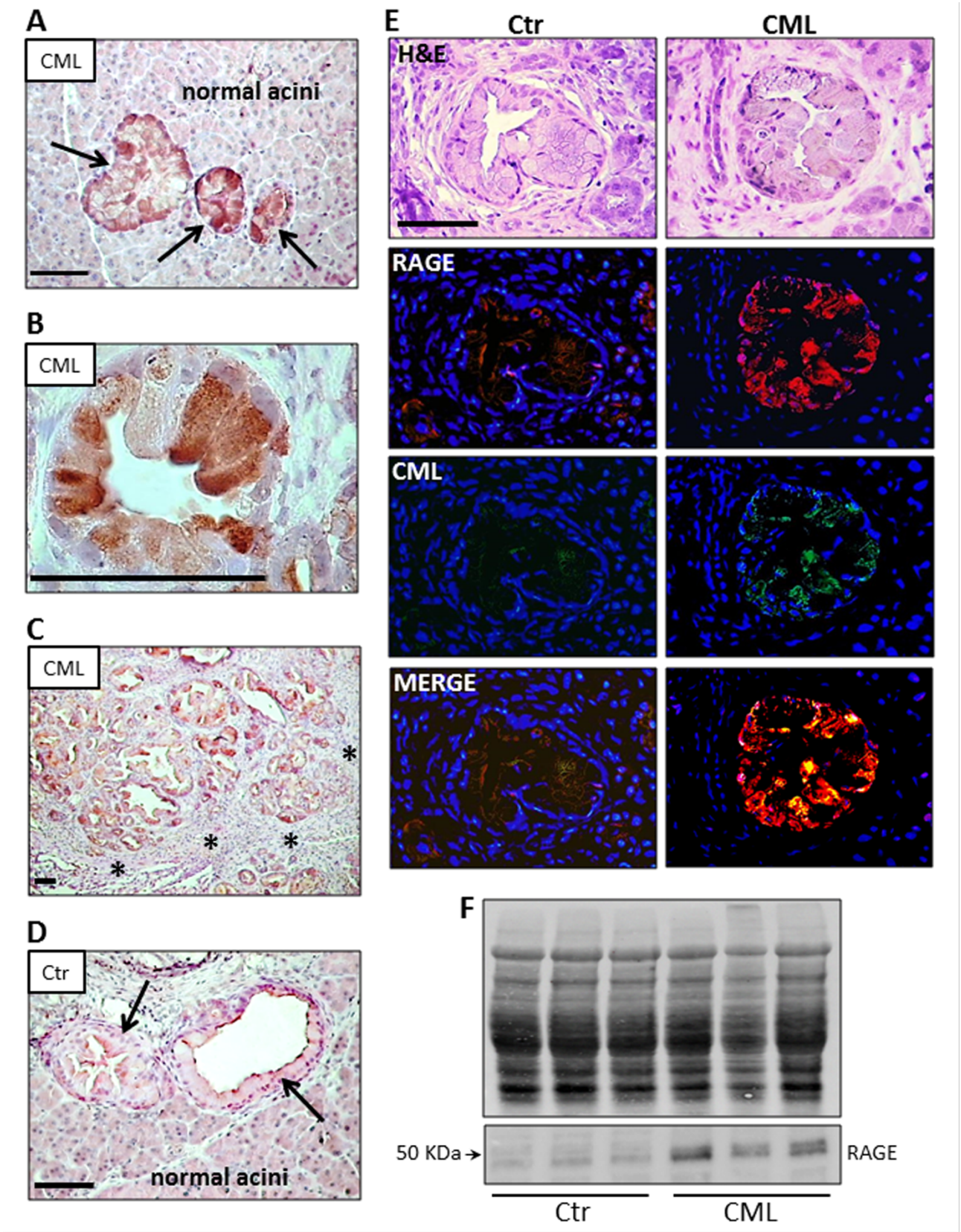
A
CML
normal acini
B
CML
C
CML
D
Ctr
normal acini
E
Ctr
CML
H&E
RAGE
CML
MERGE
F
50 KDa
RAGE
Ctr
CML

Figure 5

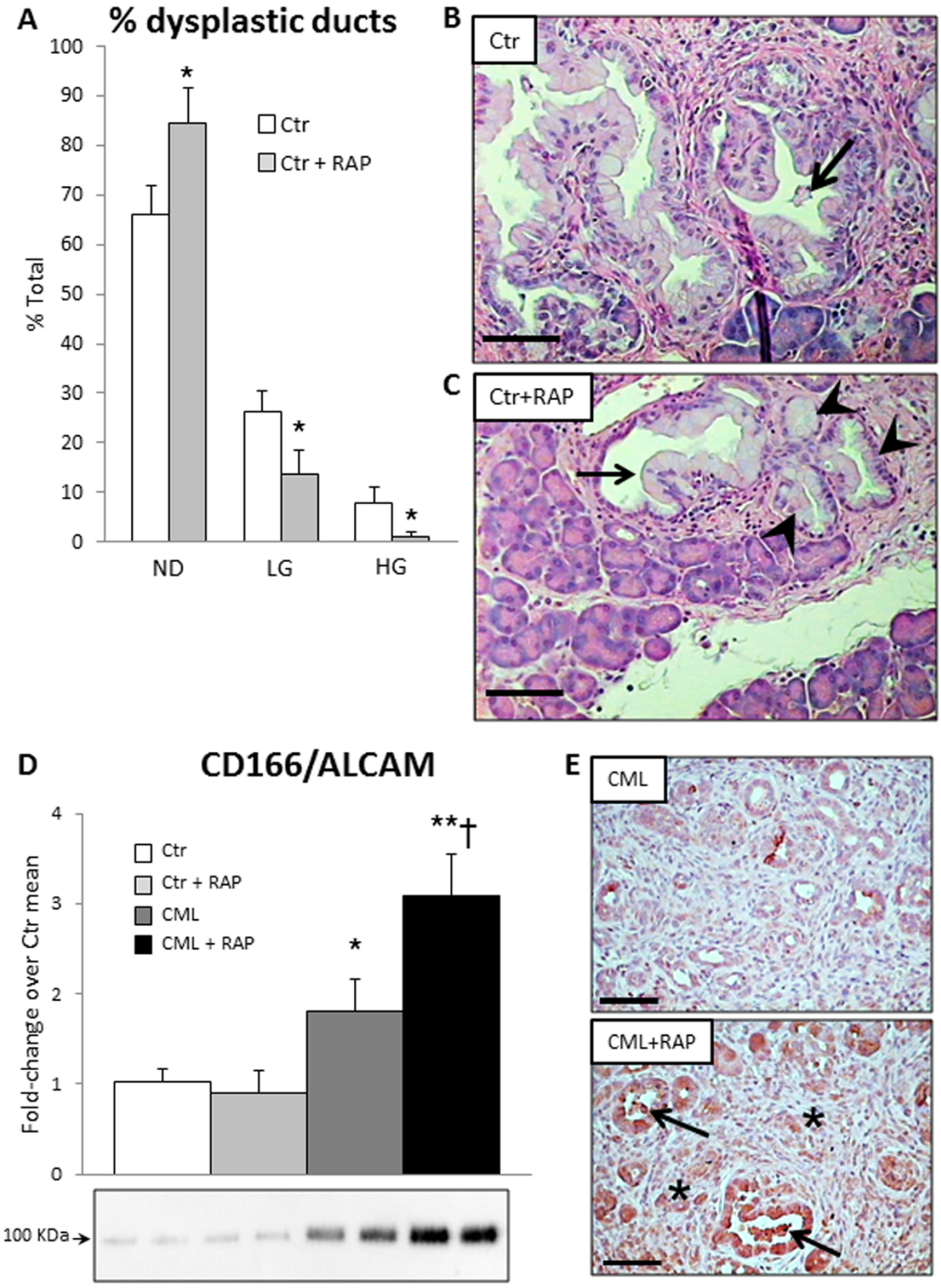
A
% dysplastic ducts
100
90
80
70
60
50
40
30
20
10
0
% Total
*
*
*
Ctr
Ctr + RAP
ND
LG
HG
B
Ctr
C
Ctr+RAP
D
CD166/ALCAM
4
3
2
1
0
Fold-change over Ctr mean
Ctr
Ctr + RAP
CML
CML + RAP
*
**†
100 KDa
E
CML
CML+RAP
*
*

Figure 6

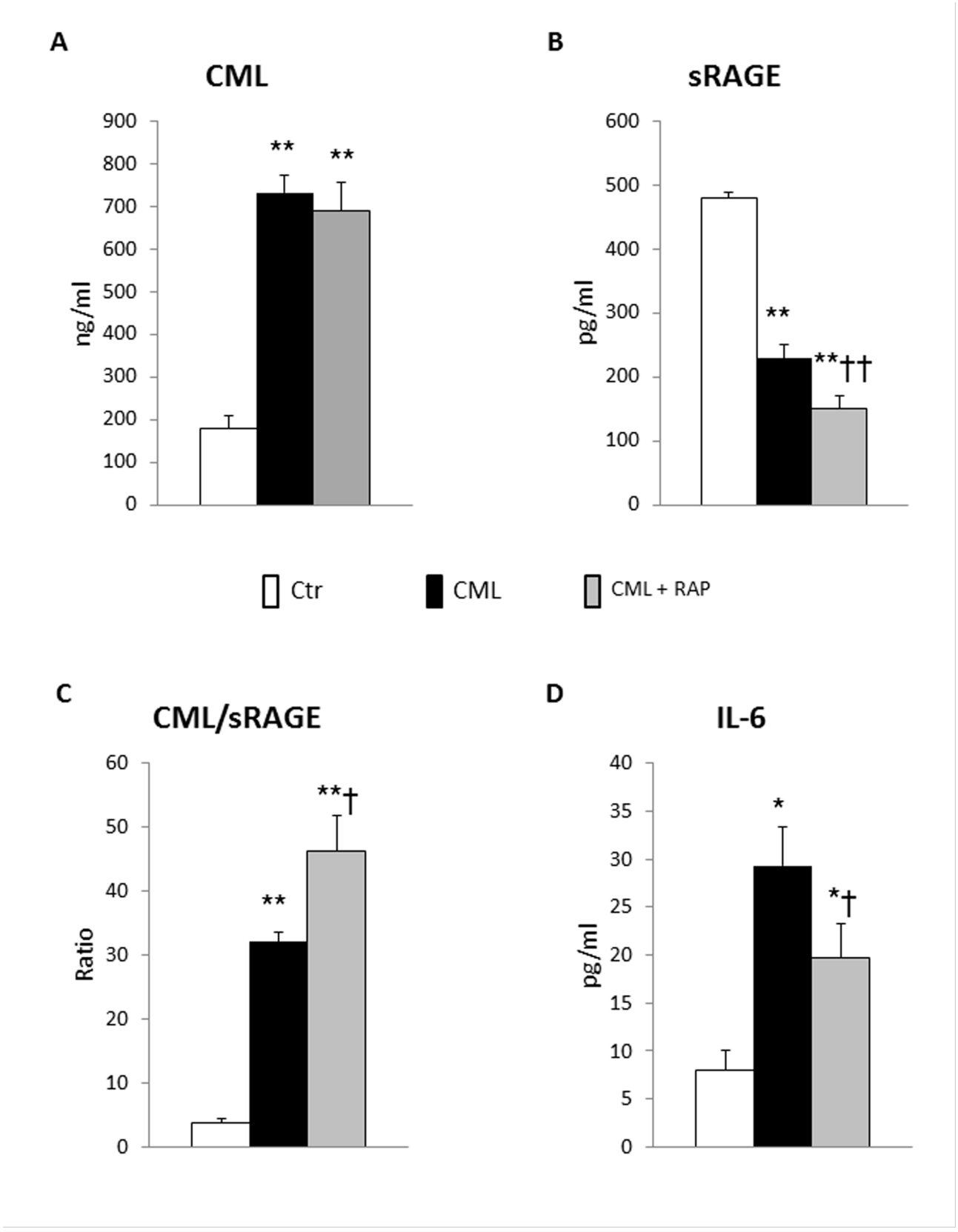
A
CML
ng/ml
900
800
700
600
500
400
300
200
100
0
**
**
B
sRAGE
pg/ml
600
500
400
300
200
100
0
**
**††
Ctr
CML
CML + RAP
C
CML/sRAGE
Ratio
60
50
40
30
20
10
0
**
**†
D
IL-6
pg/ml
40
35
30
25
20
15
10
5
0
*
*†

Supporting information

Supplementary Methods

Supplementary Table 1. TaqMan Gene Expression assays.

Supplementary Table 2. Antibodies used in Western blot and IHC studies.

Supplementary Table 3. Primers for genotyping.

Supplementary Figure 1. Analysis of the binding of RAGE to immobilized CML-MSA in a functional ELISA.

Supplementary Figure 2. Validation of the ELISA kits for the determination of sRAGE and CML serum levels.

Supplementary Figure 3. HIF-1α and NFATc1 nuclear protein levels, HIF-1α DNA-binding activity and IL-6 mRNA expression in Mia PaCa-2 cells.

Supplementary Figure 4. Activation of NF-κB/p65 and PDA cell proliferation induced by CML is dependent on interaction with RAGE.

Supplementary Figure 5. *In vivo* BLI signal quantification in 11-week-old Ctr and CML-treated mice.

Supplementary Figure 6. Pancreatic protein levels of phospho (p)-STAT3.

Supplemental Figure 7. Liver and lung metastasis in KCM mice treated with CML+RAP.

Supplementary Figure 8. Stain-free membrane image for protein loading normalization relative to CD166/ALCAM Western blot.

Supplementary Methods

Reference numbers refer to the main text list

In vitro studies

Preparation and characterization of N^{ε}-(Carboxymethyl)Lysine (CML)-modified serum albumin

CML was prepared as previously reported [21,29]. Briefly, 175 mg human (HSA) or mouse (MSA) serum albumin (Sigma-Aldrich, St.Louis, MO, USA) were incubated in 1 ml of 0.2 M phosphate buffer, pH 7.8, containing 0.15 M glyoxylic acid (Sigma-Aldrich) and 0.45 M sodium cyanoborohydrate (Acros Organics, Morris Plains, NJ, USA) for 24 h at 37°C. Preparations of CML-modified albumin were extensively dialyzed versus phosphate-buffered saline (PBS) for 48 h using Cellu Sep H1 tubular membranes MWCO 15,000 (Orange Scientific, Braine l'Alleud, Belgium) purified several times through endotoxin-removing columns High Capacity Endotoxin Removal Spin Column, (Thermo Scientific, Rockford, IL, USA), passed through 22 μm filters, and assessed for endotoxin content by the Limulus amoebocyte lysate test kit (Sigma-Aldrich). Protein concentration was assessed by the Bradford assay (Bio-Rad, Hercules, CA, USA). The extent of murine (MSA) and human (HSA) lysine modification was determined by employment of 2,4,6-trinitrobenzenesulfonic acid (TNBSA) (Thermo Fisher Scientific, Waltham, MA, USA), according to manufacturer's instructions. Briefly, 250μl of TNBSA solution were added to 500 μl of each sample. After incubation at 37°C for two hours, the reaction was terminated by adding 250 μl of 10% SDS and 125 μl of 1N HCl followed by measurement of absorbance at 420 nm. The standard curve generated by unmodified HSA or MSA was used as the calibration standard.

RAGE neutralization

In order to evaluate the actual contribution of advanced glycation endproducts receptor (RAGE) in the cellular effects induced by CML-modified albumin, cells were treated with an anti-RAGE antibody to neutralize the RAGE receptors prior to CML challenge. The immunologic strategy was preferred to the RNA interference one because RNA-mediated gene silencing may induce non-specific or off-target effects such as NF-κB activation, which in turn may affect tumor cell survival

[50]. Briefly, MiaPaCa2 cells were incubated for one hour with 10 µg/mL anti-RAGE antibody (PA5-24787, Thermo Fisher Scientific) directed to the V domain of the N-terminal region of RAGE, which is the extracellular domain involved in RAGE ligation by CML [28], or 10 µg/mL IgG isotype control (#10500C Thermo Fisher Scientific). Then, cells were treated with 50 µg/ml CML for 24 h prior to evaluate cell proliferation by cell count and the DNA-binding activity of NF-κB/p65 by the TransAM NFkB p65 kit (Active Motif Corp., Carlsbad, CA, USA). Each condition was done in triplicate, and the experiment was repeated 3 times.

In vitro analysis of the binding of RAGE to immobilized CML-MSA

To confirm RAGE binding to the CML-MSA preparation, we measured its binding ability in a functional ELISA, as previously reported by Rao *et al* [51]. Polyvinyl 96-well plates were coated with 0.5 µg/well of CML-MSA or native MSA as negative control. Next, 50 µl of 0.25, 0.5 and 1 nM recombinant mouse RAGE provided as standard with the ELISA kit for sRAGE (#893192, R&D Systems, Minneapolis, MN, USA) were added to each CML-MSA or native MSA-coated well and incubated at 37°C for 1 h. To detect bound RAGE, 50 µl of the polyclonal antibody specific for mouse RAGE conjugated to horseradish peroxidase provided with the same kit (#893191, R&D Systems) was added to each well and the mixture was incubated for 1 h at room temperature. Color reagent A (#895000, R&D Systems) and B (#895001, R&D Systems) were added, reaction stopped with stop solution (#895174, R&D Systems) and the colorimetric reaction was evaluated by reading absorbance at 450 nm using an automated microplate reader (Varioskan Lux, Thermo Fischer Scientific).

***In vivo* studies**

Generation of the transgenic animal model

The *LSL-Kras*$^{G12D/+}$ lineage was maintained in the heterozygous state. Mice were screened by PCR using tail DNA amplified by specific primers to the Lox-P cassette flanking mutated *Kras*$^{G12D/+}$, wild type *Kras*, *Cre* recombinase and *MITO* genes (Supplementary Table S3).

In the *MITO-Luc* mouse, an artificial minimal promoter derived from the cyclin B2 gene and induced by NF-Y drives the expression of the luciferase reporter specifically in proliferating cells, which may therefore be localized by a bioluminescence imaging (BLI)-based screen [37,38]. We have previously shown that KCM mice develop pre-invasive (PanIN) and invasive ductal PaC with the same penetrance, latency and histological features as those described for KC mice [38].

RAGE and CML pancreatic tissue distribution

Pancreatic tissue distribution and co-localization of RAGE and CML were evaluated immunohistochemically [29,52] by dual label immunofluorescence [52] using a goat polyclonal antibody to amino acids 42-59 of human RAGE (ab7764, Abcam, Cambridge, UK), and a mouse monoclonal antibody against CML (ab27685, Abcam), as primary antibodies. Then, an Alexa Fluor®594 chicken anti-goat IgG H&L (Invitrogen, Carlsbad, CA, USA) and a DyLight®488 anti-mouse IgG H&L (Vector Labs, Burlingame, CA, USA) were used as secondary antibodies (52). Sections were analyzed at a fluorescence microscope (Zeiss AXIO A1), equipped with an Axiocam 503 color camera (Carl Zeiss Italy, Milan, Italy).

TGX Stain-Free technology for total protein measurement

For Western blot analysis, proteins were separated on a TGX Stain-Free Gel (Bio-Rad laboratories) and activated by a 2 min ultraviolet exposure using the ChemiDoc XRS+ Imager (Bio-Rad laboratories). After protein transfer, membranes were imaged for Stain-Free staining and total proteins in each lane were quantified using the ImageLab 5.2 software (Bio-Rad laboratories) and normalized using Stain-Free technology (Bio-Rad laboratories). This approach was preferred to the use of an internal standard due to the poor reliability of housekeeping proteins, which showed significant variations, especially between samples with and without invasive neoplastic disease.

Validation of ELISA kits for the determination of sRAGE and CML serum levels

In order to verify whether the presence of CML in the assay system could affect sRAGE data obtained by ELISA, CML-MSA was added to pooled serum from three Ctr mice at a final concentration of 300, 600, or 900 ng/ml prior to assess sRAGE level with mouse sRAGE ELISA kit (R&D Systems). The same pooled serum with equal volume of PBS added was used as control. The same procedure was used to evaluate the potential interference of the RAGE antagonist peptide (RAP) with sRAGE data. In this case, RAP (Calbiochem, Merck KGaA, Darmstadt, Germany) was added to pooled serum at a final concentration of 5, 10, or15 μM. The range of final concentrations of CML-MSA was comparable to that of CML serum levels detected in CML-treated KCM mice, whereas that of RAP comprised the concentration used in the *in vitro* experiments (10 μM), which was shown to be able to block RAGE activity. We also verified whether the presence of sRAGE or RAP in the CML assay system could affect CML data obtained by ELISA. For this purpose, RAGE (#893192, R&D Systems) or RAP were added to pooled serum from three CML mice prior to assessing CML levels with CML ELISA kit (R&D Systems). The final concentration of RAGE was 100, 300, or 600 pg/ml, i.e., within the range of circulating RAGE levels detected in mice. The final concentration of RAP was 5, 10, or15 μM, as reported above. The same pooled serum with equal volume of PBS added was used as control.

Table S1. TaqMan Gene Expression assays

Target	Assay
AGER	Hs00153957_m1
ALCAM	Hs00977641_m1
NFATC1	Hs00542678_m1
PIM1	Hs01065498_m1
IL6	Hs00174131_m1

AGER = receptor for advanced glycation endproducts; *ALCAM* = activated leukocyte cell adhesion molecule; *NFATC1* = nuclear factor of activated T-cells cytoplasmic 1; *PIM1* = serine/threonine-protein kinase Pim-1; *IL6* = interleukin-6.

Table S2. Antibodies used in Western blot and IHC studies.

Target	Antibody	Catalog Nr.	Supplier
Primary			
NF-κB subunit p65	mouse monoclonal F-6	SC8008	Santa Cruz Biotechnology, Dallas, TX, USA
(p)STAT3	rabbit polyclonal	9131S	Cell Signaling Technology, Danvers, MA, USA
STAT3	rabbit monoclonal 79D7	4904	Cell Signaling Technology, Danvers, MA, USA
NFATC1	mouse monoclonal	MAB3209	Abnova, Taipei City, Taiwan
HIF-1α	rabbit monoclonal	ab51608	Abcam, Cambridge, UK
RAGE (IHC)	goat polyclonal	ab7764	Abcam, Cambridge, UK
RAGE (WB)	rabbit polyclonal	PA5-24787	Thermo Fisher Scientific, Waltham, MA, USA
CML	goat polyclonal	ab27685	Abcam, Cambridge, UK
CD166/ALCAM (WB & IHC)	rabbit monoclonal EPR2759(2)	ab1092015	Abcam, Cambridge, UK
Secondary			
HIF-1α, RAGE (WB), CD166/ ALCAM (WB)	HRP-conjugated goat anti-rabbit	P0448	Agilent/Dako, Santa Clara, CA, USA
NF-κB subunit p65, NFATC1	HRP-conjugated goat anti-mouse HRP conjugated	P0447	Agilent/Dako, Santa Clara, CA, USA
RAGE (IHC/IP)	Biotinylated rabbit anti-goat IgG	ab6740	Abcam, Cambridge, UK
CD166/ALCAM (IHC)	Biotinylated goat anti-rabbit IgG	E0432	Agilent/Dako, Santa Clara, CA, USA
RAGE (IHC/IF)	Alexa Fluor® 594 chicken anti-goat IgG	A-21468	Invitrogen, Carlsbad, CA, USA
CML	DyLight®488 horse anti-goat IgG	DI-3088	Vector Laboratories, Burlingame, CA, USA

WB = Western blot; IHC = immunohistochemistry; NF-κB = nuclear factor-κB; p-STAT3 = phosphorylated Signal Transducer and Activator of Transcription 3; NFATC1 = nuclear factor of

activated T-cells cytoplasmic 1; HIF-1 = hypoxia-inducible factor 1; RAGE = receptor for advanced glycation endproducts; CML = N^{ε}-carboxymethyl lysine; ALCAM = activated leukocyte cell adhesion molecule; IP = immunoperoxidase; IF = immunofluorescence.

Table S3. Primers for genotyping.

Gene	Oligonucleotide	Primer
Kras	Oligonucleotide 1:	5'-GTCTTTCCCCAGCACAGTGC;
	Oligonucleotide 2:	5'-CTCTTGCCTACGCCACCAGCTC;
	Oligonucleotide 3:	5'-AGCTAGCCACCATGGCTTGAGTAAGTCTGCA.
Pdx-1-	Oligonucleotide up:	5'-ATGCTTCTGTCCGTTTGCCG;
Cre	Oligonucleotide	5'-TGAGTGAACGAACCTGGTCG.
	down:	
MITO	Oligonucleotide up:	5'-
	Oligonucleotide	TGTAGACAAGGAAACAACAAAGCCTGGTGGCC;
	down:	5'-GGCGTCTTCCATTTTACCAACAGTACCGG.

Supplementary Figures

Figure S1. Analysis of the binding of RAGE to immobilized CML-MSA in a functional ELISA. 50 µl of 0.25, 0.5 and 1 nM of mouse RAGE/Fc chimera were added to wells coated with 0.5 µg of CML-MSA or native MSA and incubated at 37°C for 1 h. RAGE bound immobilized CML-MSA in a dose-dependent manner, at variance with native MSA. Data are means±SD of triplicate wells for each concentration of mouse RAGE/Fc chimera. Two-tailed test: *P< 0.001 vs. MSA.

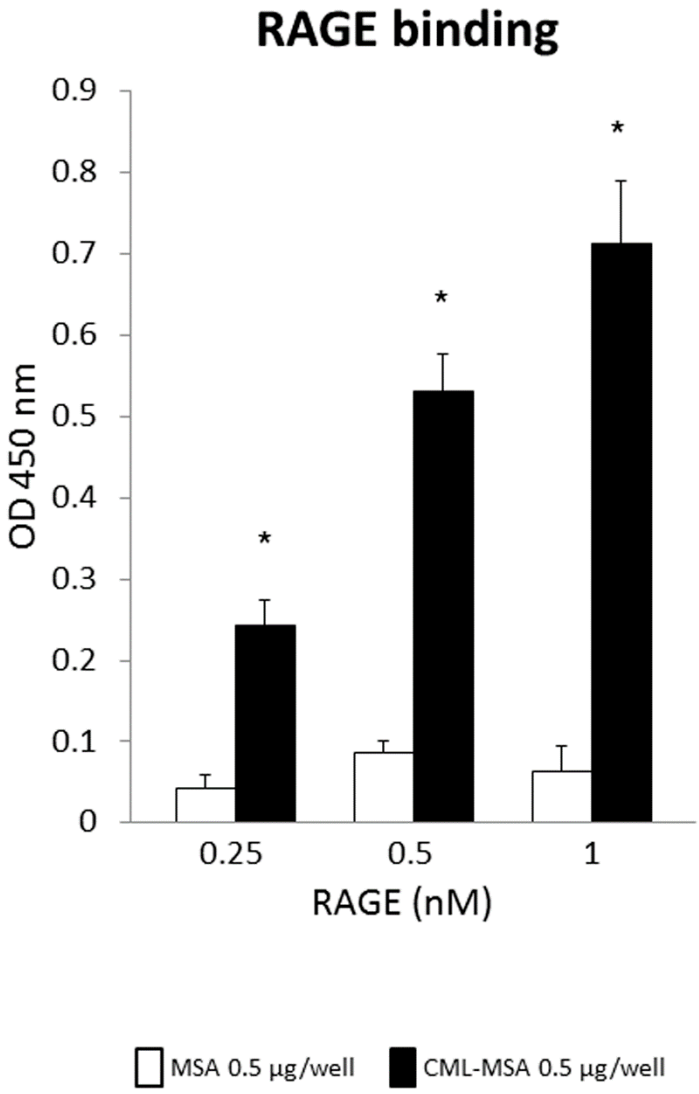

Figure S2. Validation of the ELISA kits for the determination of sRAGE and CML serum levels. Data on serum sRAGE (A,B) levels detected by ELISA in pooled serum from three Ctr mice were not affected by the addition of increasing amounts of CML (A) or RAP (B) in the assay system. Likewise, serum CML levels (C,D) detected by ELISA in pooled serum from three CML mice were not affected by the addition of increasing amounts of sRAGE (C) or RAP (D). Data are means±SD of triplicate wells per condition.

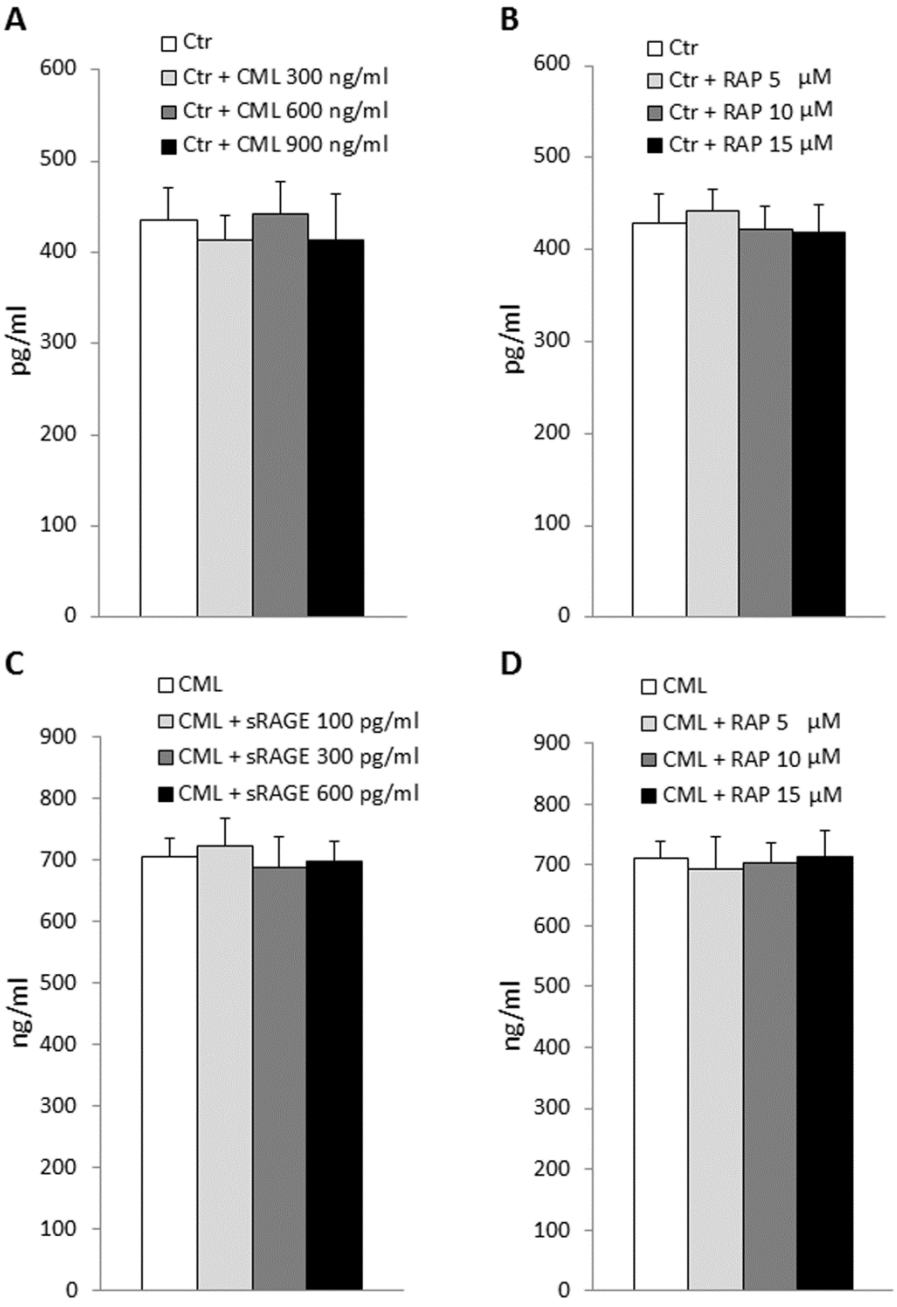

Figure S3. HIF-1α and NFATc1 nuclear protein levels, HIF-1α DNA-binding activity and IL-6 mRNA expression in Mia PaCa-2 cells. (A) Representative Western blot for NFATc1 and HIF-1α nuclear protein levels in Mia PaCa-2 cells exposed to native HSA (Ctr), CML-modified HSA (CML) or CML+RAP at the concentration indicated for 24 h and relative band densitometry analysis from three separate experiments. (B) ELISA for DNA-binding activity of HIF-1α and *IL6* mRNA expression in Mia PaCa-2 cells exposed to 50 µg/ml of HSA or CML, and 50 µg/ml CML plus 10 µmol/L of RAP for 24 h. Nuclear extract from HeLa cells treated with CoCl2 is provided as positive control for HIF-1 activation by the manufacturer. Data represent three separate experiments. Post-hoc multiple comparison: *P< 0.05, **P<0.01 and ***P<0.001 vs. HSA; †P<0.05 ††P<0.01 and †††P<0.001 vs. CML.

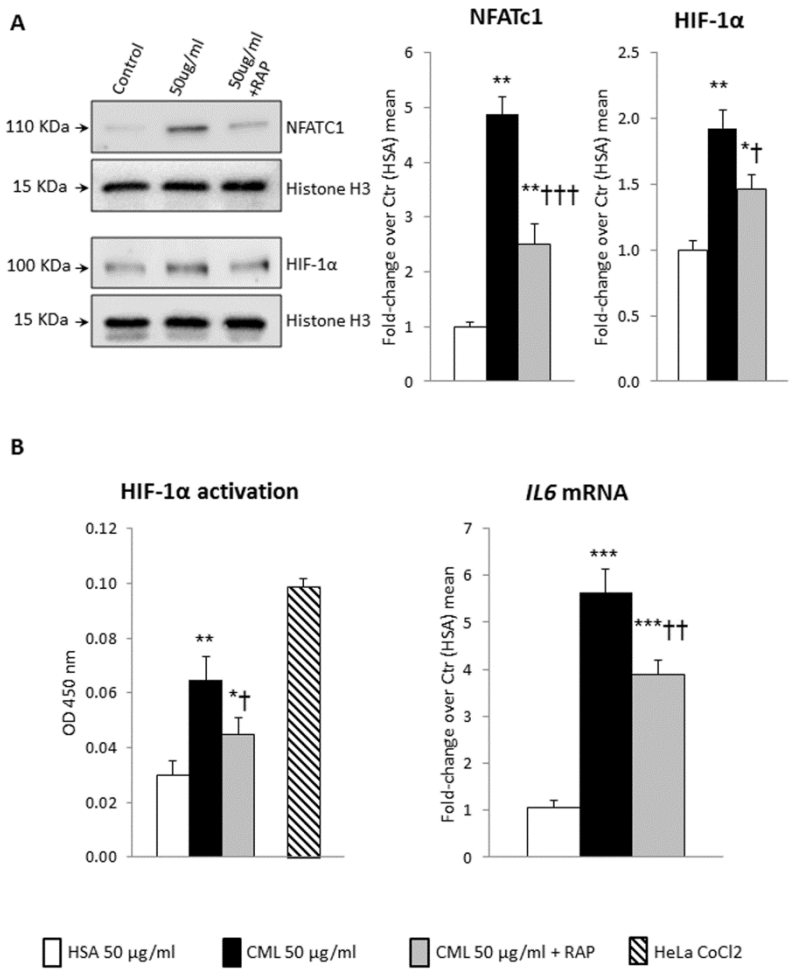

Figure S4. Activation of NF-κB/p65 and PDA cell proliferation induced by CML is dependent on interaction with RAGE. (A) NF-κB/p65 activity of the nuclear extracts assessed by ELISA and (B) cell proliferation in MIA PaCa-2 cells incubated for one hour with 10 µg/mL anti-RAGE antibody or 10 µg/mL IgG isotype control and exposed to 50 µg/ml of CML for 24h; n = 3 wells per condition. Post-hoc multiple comparison: *P<0.001 vs. HSA; †P< 0.01 vs CML + IgG control.

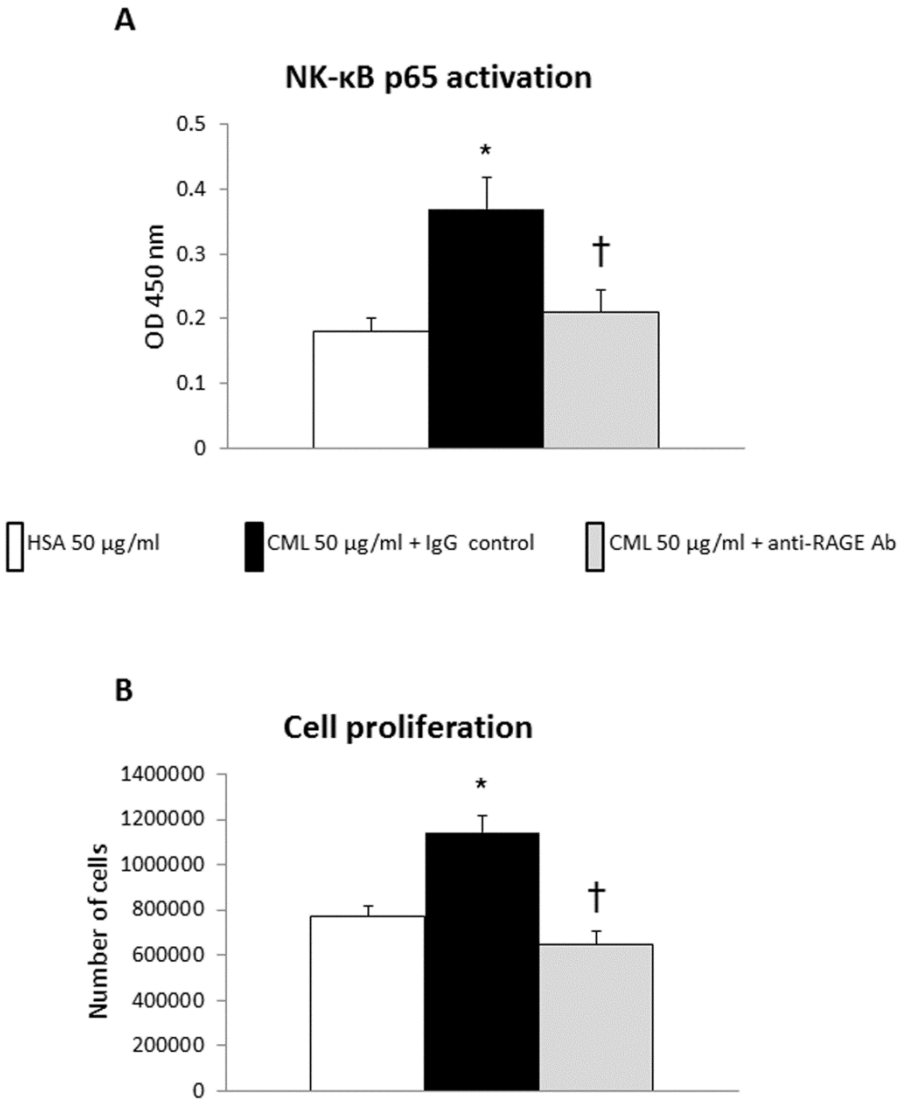

Figure S5. *In vivo* BLI signal quantification in 11-week-old Ctr and CML-treated mice. Box plots represent *in vivo* BLI signal quantification in Ctr (n=11) and CML-treated (n=11) KCM mice. Data were expressed as photon/second/cm^2/steradiant (p/s/cm2/sr).

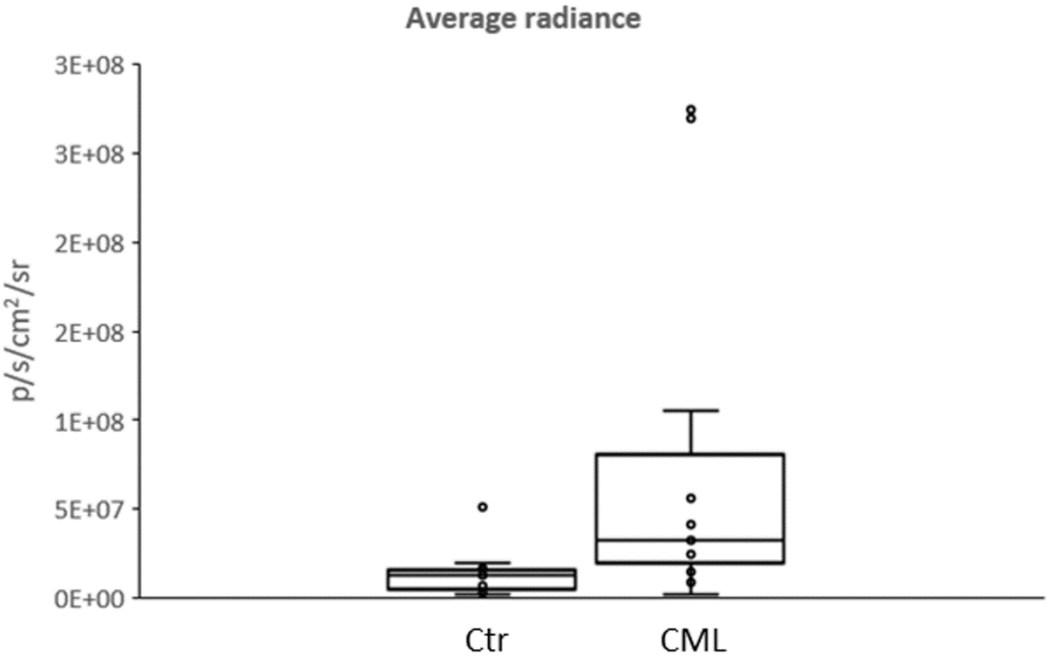

Figure S6. Pancreatic protein levels of phospho (p)-STAT3. Representative Western blot for STAT3 protein phosphorylation in three Ctr and three CML-treated KCM mice and relative band densitometry analysis from five mice per group. The membrane used for RAGE detection was reprobed with anti-STAT 3 antibody after stripping. Therefore, normalization for total protein content was performed on the same Stain-Free gel (upper box) used for RAGE normalization (see Figure 4E). The lower boxes show acquisition of the immunoreactive p-STAT3 and total STAT3 bands. Two-tailed test: *P< 0.001 vs. Ctr.

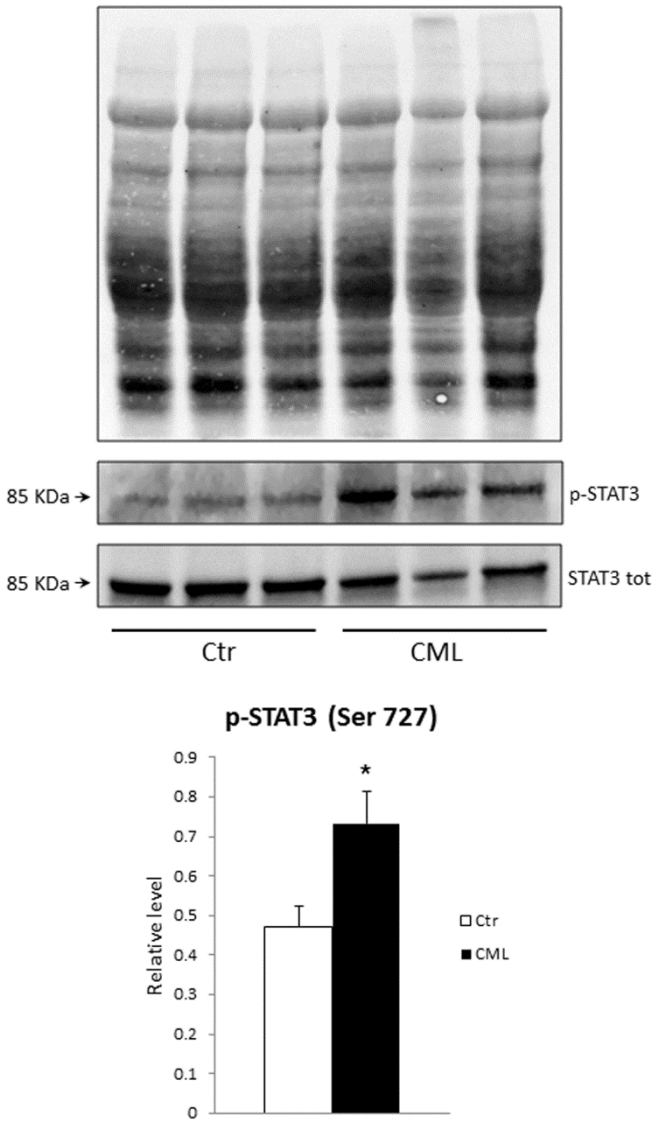

Figure S7. Liver and lung metastasis in KCM mice treated with CML+RAP. (A) A large, well differentiated liver metastasis. Cells were arranged in ductal-like structures (arrows). CV = central vein. (B) Lung, undifferentiated metastasis surrounded by dashed line. Scale bar = 100µm

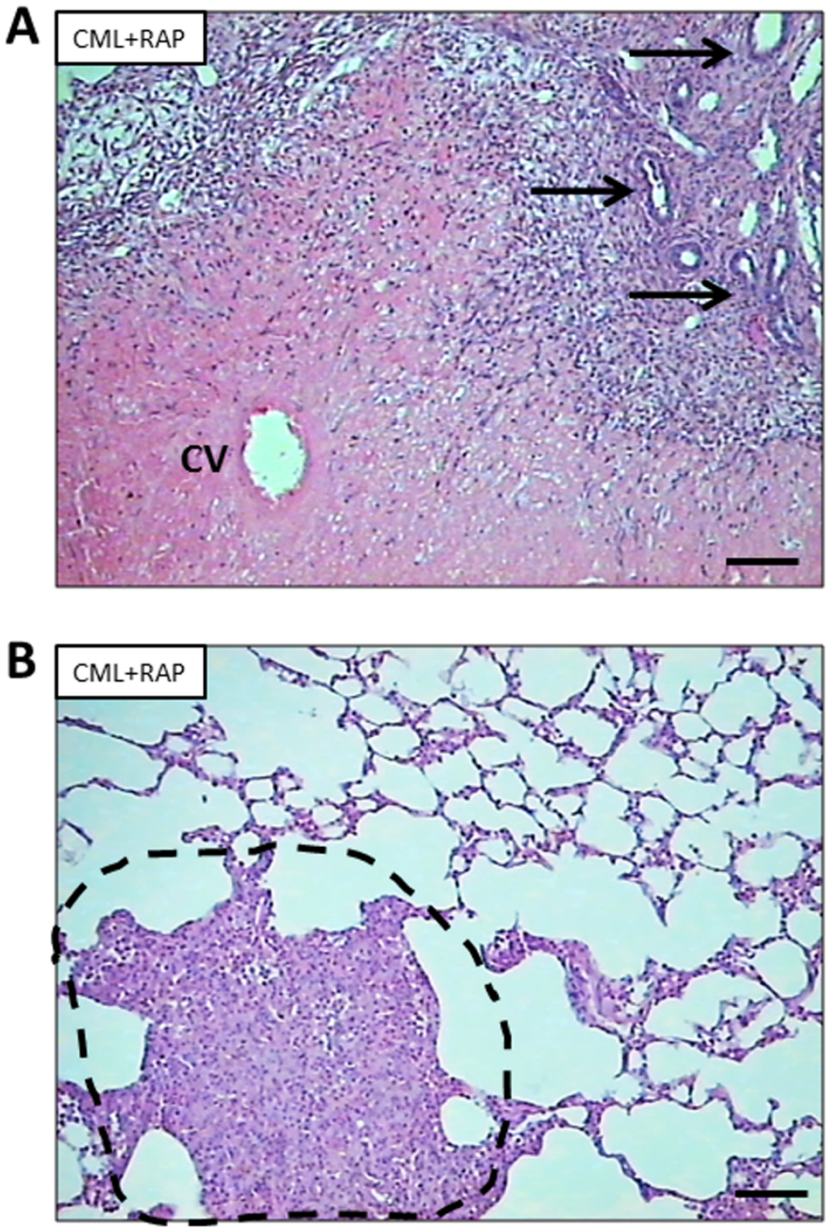

Figure S8. Stain-free membrane image for protein loading normalization relative to CD166/ALCAM Western blot. Acquisition of total protein content after Stain-Free gel exposure to ultraviolet light and protein transfer onto a nitrocellulose membrane for CD166/ALCAM Western blot normalization (see Figure 5D).